

NASA TECHNICAL NOTE



NASA TN D-3591

2.1



TECH LIBRARY KAFB, NM

0077994

10 OCT 1966
RECEIVED
AF V CARPENS
LABORATORY

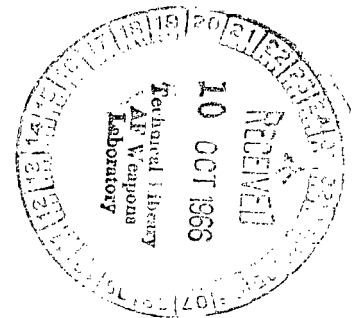
NASA TN D-3591

STATIC AND DYNAMIC LONGITUDINAL STABILITY DERIVATIVES OF A POWERED 1/9-SCALE MODEL OF A TILT-WING V/STOL TRANSPORT

by Joseph R. Chambers and Sue B. Grafton

Langley Research Center

Langley Station, Hampton, Va.





0079994

NASA TN D-3591

STATIC AND DYNAMIC LONGITUDINAL STABILITY DERIVATIVES OF A
POWERED 1/9-SCALE MODEL OF A TILT-WING V/STOL TRANSPORT

By Joseph R. Chambers and Sue B. Grafton

Langley Research Center
Langley Station, Hampton, Va.

NATIONAL AERONAUTICS AND SPACE ADMINISTRATION

For sale by the Clearinghouse for Federal Scientific and Technical Information
Springfield, Virginia 22151 – Price \$2.00

STATIC AND DYNAMIC LONGITUDINAL STABILITY DERIVATIVES OF A POWERED 1/9-SCALE MODEL OF A TILT-WING V/STOL TRANSPORT

By Joseph R. Chambers and Sue B. Grafton
Langley Research Center

SUMMARY

Static and oscillatory force tests were conducted to determine the power-on longitudinal stability derivatives of a model of a tilt-wing V/STOL transport aircraft. The model had four propellers and the wing could be tilted from an incidence of 0° (for conventional forward flight) to 90° (for hovering flight). The investigation consisted of tests at several wing incidence angles and thrust conditions for an angle-of-attack range of $\pm 30^\circ$. The forced oscillation equipment and dynamic data readout system are also described.

The results indicate that the model was statically unstable for wing incidence angles above about 15° but was stable for lower angles. The model had positive damping in pitch (negative values of the damping-in-pitch parameter $MY_q + MY_{\dot{\alpha}}$) throughout the conditions investigated.

INTRODUCTION

The interest in tilt-wing V/STOL aircraft has become so substantial that there now exists a need to obtain representative data for detailed dynamic stability analysis during the design stages of such vehicles. There is at the present time very little information available correlating estimated and experimentally measured dynamic stability derivatives of tilt-wing configurations. The present investigation was therefore undertaken to supply some experimentally measured static and dynamic longitudinal stability derivatives of a typical tilt-wing configuration. The model used in this investigation was a 1/9-scale model of a four-propeller tilt-wing V/STOL transport. The results of free-flight tests of the model are presented in reference 1.

The investigation covered a range of angle of attack from -30° to 30° and a range of wing incidence angle from 0° (wing positioned for conventional forward flight) to 90° (wing positioned for hovering flight). All tests were made for several thrust conditions inasmuch as it was expected that thrust conditions would greatly affect the measured static and dynamic stability derivatives.

SYMBOLS AND NOMENCLATURE

All quantities with the exception of lift and drag are presented with respect to the system of body axes shown in figure 1. Inasmuch as conventional nondimensional coefficients lose their significance and tend to become infinite as the airspeed approaches zero, a major portion of the damping data is presented in dimensional form. Dimensional values are given both in U.S. Customary Units and in the International System of Units (SI). Factors relating the two systems are given in reference 2. Included in each presentation of data are the values of the nondimensionalizing parameters required for converting the data to standard coefficient form.

c	chord length, feet (meters)
\bar{c}	mean aerodynamic chord, feet (meters)
E	strain-gage supply voltage, volts
E_{in}	voltage in phase with displacement, volts
E_{out}	voltage out of phase with displacement, volts
E_R	amplitude of resolver voltage, volts
e_m	voltage proportional to pitching moment, volts
e_x	voltage proportional to longitudinal force, volts
e_z	voltage proportional to vertical force, volts
F_X	force along X body axis, pounds (newtons)
F_Z	force along Z body axis, pounds (newtons)
f	frequency of oscillation, cycles per second
I_Y	moment of inertia about Y body axis, slug-feet ² (kilogram-meters ²)
i_t	tail incidence angle, degrees

i_w	wing incidence angle, degrees
k	reduced frequency parameter, $\omega \bar{c}/2V$
k_m	balance calibration factor, volts output per volt-foot-pound (volts output per volt-meter-newton)
L_0	value of lift for longitudinal acceleration equal to zero at an angle of attack of 0° , pounds (newtons)
M_Y	pitching moment, foot-pounds (meter-newtons)
M_{Y_0}	static pitching moment at mean angle of attack of oscillation, foot-pounds (meter-newtons)
q	pitching velocity, radians per second
Δq	pitching velocity increment, radians per second
q_∞	free-stream dynamic pressure, $\rho V^2/2$, pounds per square foot (newtons per square meter)
S	wing area, square feet (square meters)
T	period of oscillation, seconds
t	time, seconds
t_0	reference time, seconds
V	free-stream velocity, feet per second (meters per second)
W	weight, pounds (newtons)
W/S	wing loading, pounds per square foot (newtons per square meter)
X, Y, Z	body reference axes (see fig. 1)
α	angle of attack, degrees or radians

$\Delta\alpha$	angle-of-attack increment, degrees or radians
$\Delta\alpha_{\max}$	amplitude of incremental angle of attack during oscillation, degrees or radians
δ_f	flap deflection, degrees
θ	pitch angle, herein defined as angular displacement of X body axis from wind-tunnel center line, radians
$\Delta\theta$	pitch-angle increment, radians
$\Delta\theta_{\max}$	amplitude of incremental pitch angle during oscillation, degrees or radians
ρ	air density, slugs per cubic foot (kilograms per cubic meter)
ω	angular velocity, $2\pi f$, radians per second

$$F_{X\alpha} = \frac{\partial F_X}{\partial \alpha} \qquad F_{Z\alpha} = \frac{\partial F_Z}{\partial \alpha} \qquad M_{Y\alpha} = \frac{\partial M_Y}{\partial \alpha}$$

$$F_{X\dot{\alpha}} = \frac{\partial F_X}{\partial \dot{\alpha}} \qquad F_{Z\dot{\alpha}} = \frac{\partial F_Z}{\partial \dot{\alpha}} \qquad M_{Y\dot{\alpha}} = \frac{\partial M_Y}{\partial \dot{\alpha}}$$

$$F_{Xq} = \frac{\partial F_X}{\partial q} \qquad F_{Zq} = \frac{\partial F_Z}{\partial q} \qquad M_{Yq} = \frac{\partial M_Y}{\partial q}$$

$$F_{X\dot{q}} = \frac{\partial F_X}{\partial \dot{q}} \qquad F_{Z\dot{q}} = \frac{\partial F_Z}{\partial \dot{q}} \qquad M_{Y\dot{q}} = \frac{\partial M_Y}{\partial \dot{q}}$$

$$C_X = \frac{F_X}{q_\infty S} \qquad C_Z = \frac{F_Z}{q_\infty S} \qquad C_m = \frac{M_Y}{q_\infty S \bar{c}}$$

$$C_D = \frac{\text{Drag}}{q_\infty S} \qquad C_L = \frac{\text{Lift}}{q_\infty S} \qquad M_{YV} = \frac{\partial M_Y}{\partial V}$$

$$C_{X\alpha} = \frac{\partial C_X}{\partial \alpha} \qquad C_{Z\alpha} = \frac{\partial C_Z}{\partial \alpha} \qquad C_{m\alpha} = \frac{\partial C_m}{\partial \alpha}$$

$$C_{X\dot{\alpha}} = \frac{\partial C_X}{\partial \frac{\dot{\alpha}\bar{c}}{2V}}$$

$$C_{Z\dot{\alpha}} = \frac{\partial C_Z}{\partial \frac{\dot{\alpha}\bar{c}}{2V}}$$

$$C_{m\dot{\alpha}} = \frac{\partial C_m}{\partial \frac{\dot{\alpha}\bar{c}}{2V}}$$

$$C_{Xq} = \frac{\partial C_X}{\partial \frac{q\bar{c}}{2V}}$$

$$C_{Zq} = \frac{\partial C_Z}{\partial \frac{q\bar{c}}{2V}}$$

$$C_{mq} = \frac{\partial C_m}{\partial \frac{q\bar{c}}{2V}}$$

$$C_{X\dot{q}} = \frac{\partial C_X}{\partial \frac{\dot{q}\bar{c}^2}{4V^2}}$$

$$C_{Z\dot{q}} = \frac{\partial C_Z}{\partial \frac{\dot{q}\bar{c}^2}{4V^2}}$$

$$C_{m\dot{q}} = \frac{\partial C_m}{\partial \frac{\dot{q}\bar{c}^2}{4V^2}}$$

A dot over a symbol represents a derivative with respect to time.

In the present investigation the term "in-phase derivative" refers to any one of the oscillatory derivatives that is based on the components of forces and moments in phase with the angle of pitch produced in the oscillatory tests. The term "out-of-phase derivative" refers to any one of the stability derivatives that is based on the components of forces and moments 90° out of phase with the angle of pitch. The oscillatory derivatives of the present investigation were measured in the following combinations:

Nondimensional

In phase	Out of phase
$C_{m\alpha} - k^2 C_{m\dot{q}}$	$C_{mq} + C_{m\dot{\alpha}}$
$C_{Z\alpha} - k^2 C_{Z\dot{q}}$	$C_{Zq} + C_{Z\dot{\alpha}}$
$C_{X\alpha} - k^2 C_{X\dot{q}}$	$C_{Xq} + C_{X\dot{\alpha}}$

Dimensional

In phase	Out of phase
$M_{Y\alpha} - \omega^2 M_{Y\dot{q}}$	$M_{Yq} + M_{Y\dot{\alpha}}$
$F_{Z\alpha} - \omega^2 F_{Z\dot{q}}$	$F_{Zq} + F_{Z\dot{\alpha}}$
$F_{X\alpha} - \omega^2 F_{X\dot{q}}$	$F_{Xq} + F_{X\dot{\alpha}}$

TEST EQUIPMENT AND TECHNIQUE

Tunnel

All tests were made in the open throat test section of the Langley full-scale tunnel. The model was mounted about 10 feet (3.05 m) above the ground board during the tests. No corrections for flow angularity or blockage have been applied to the data, since these effects were believed to be small.

Model

A photograph of the tilt-wing model used in this investigation is presented in figure 2. A three-view sketch showing some of the more important model dimensions is presented in figure 3. Geometric characteristics of the model are listed in table I.

The four main propellers were interconnected by a system of shafts and gearboxes. Compressed air was used to power both the main propellers and the tail rotor through separate pneumatic motors. The wing could be rotated through an incidence range of 0° to 90° by means of an electric motor. The wing was equipped with slats along the portions of the leading edge which were behind the up-going propeller blades; and the wing was also fitted with a double-slotted flap whose geometric characteristics are shown in figure 4. The flap was programed with a cam and follower to deflect as wing incidence changed. The variation of flap deflection angle with wing incidence angle is shown in figure 5. Also shown in figure 5 is the programed variation of the incidence of the all-movable horizontal tail. Wing-fuselage ramps were used to improve the airflow in the area of the wing center section as the wing incidence was changed. Additional information relating to the model can be found in reference 1.

Apparatus

All force tests were made with a single strut or sting support system and strain-gage balances. The static force tests were made with the model mounted on a conventional sting which entered the rear of the fuselage. The forced oscillation tests were made with the equipment sketched in figure 6. During the rigidly forced oscillation tests the model was mounted with its wings in a vertical plane. The strain-gage balance to which the model was attached was mounted in a steel C-channel which was allowed a single degree of rotational freedom in a yoke-pivot assembly. The C-channel was forced to oscillate about a vertical axis by a 3-horsepower variable-speed electric motor and flywheel which were mounted directly on the vertical support column. The rotary motion of the flywheel was transformed into oscillatory motion by the vertical and horizontal connecting rods which were joined by a bellcrank. The amplitude of the oscillatory motion (limited to $\pm 30^{\circ}$) was adjusted by varying the location of the lower pivot point of the vertical connecting

rod along the radius of the flywheel. The frequency of the oscillatory motion (limited to about 2 cycles per second) was varied by changing the frequency of the input electric power to the electric motor.

A precision sine-cosine potentiometer, which generated voltage signals proportional to the sine and cosine of the flywheel rotation angle, was coupled directly to the flywheel shaft and provided electrical signals proportional to the angular displacement and angular velocity of the model. These signals were used in the data readout procedure, which is described in detail in the appendix of this report.

Compressed air for the pneumatic motors was supplied through flexible plastic tubing which was attached to the model as close as possible to the moment center so as to minimize air pressure inputs to the data. The air supply was varied remotely and pressure gages were used to hold a constant power input during any given test. Angle of attack was varied by rotating the vertical support column, which was mounted on a motor-driven turntable. In addition, a switch system made it possible to refer the balance return signals to either the dynamic readout system or a static readout system.

Forced Oscillation Test Procedure

The test procedure used in the forced oscillation tests can best be explained by describing a typical test. With the model statically set at an angle of attack of 0° (non-oscillatory), the tunnel airspeed was brought up to the desired velocity. The strain-gage-balance return signals were switched to the static readout equipment, and the compressed air power for the model propellers was then increased until the net longitudinal force was zero for that particular wing incidence angle. The balance outputs were switched to the dynamic readout equipment and the model was oscillated at the desired frequency. The data acquisition process was then begun by a single pushbutton operation. Following data readout, the model angle of attack was changed by rotating the motor-driven turntable.

The aerodynamic forces and moments at the desired test condition were taken to be the difference between the wind-on, power-on and the wind-off, power-off measurements. This procedure is used to take out the effects of inertia, and there are two points that should be inferred from the procedure. First, the in-phase forces and moments presented are the aerodynamic forces alone, since the effects of inertia which were present both with the wind on and wind off in still air are excluded by the subtraction; and second, in the process of subtracting the effects of inertia from the in-phase forces and moments, a certain amount of aerodynamic forces and moments which correspond to the still-air aerodynamic damping were also subtracted. Still-air damping has not been important with conventional aircraft because the still-air damping is usually an insignificant percentage of the wind-on aerodynamic damping, but for V/STOL aircraft at very low airspeeds, or in hovering, this factor may become significant.

TESTS

The static and oscillatory force tests were made for an angle-of-attack range of -30° to 30° for wing incidence angles of 10° , 25° , 50° , and 65° . The tests were made by setting the wing incidence and varying the angle of attack while holding a constant air-speed and a constant power input to the model propellers. Additional static tests were conducted with a wing incidence angle of 90° to determine the longitudinal stability derivatives of the configuration in hovering flight (variation of forces and moments with velocities along the X and Z body axes).

A model cross-shafting failure eliminated the possibility of obtaining any power-on data for a wing incidence angle of 0° ; however, static and oscillatory tests were conducted for a wing incidence angle of 0° with propellers windmilling for an angle-of-attack range of -10° to 20° . The damping data obtained during this phase of the investigation are believed to be applicable to the trimmed level flight condition at a wing incidence of 0° .

The forced oscillation tests were made with an oscillatory amplitude of $\pm 5^{\circ}$. The range of oscillation frequencies was from 0.2 to 1.4 cycles per second. The frequency of the oscillation was held constant for a wing incidence of 65° and the reduced frequency parameter k was held constant for the other incidence angles investigated. (It is believed that the reduced frequency parameter k loses significance for very low speeds; the period of the oscillation was therefore held constant.) The location of the moment reference center for all tests is given as a function of wing incidence angle in figure 7. These locations correspond to the center-of-gravity locations of the model during the free-flight tests of reference 1. During all tests the main propeller blades were set at an angle of 12° at the 0.75 radius location. The tail rotor blades were maintained at a blade angle of 0° during the investigation.

The primary purpose of the forced oscillation tests was to determine the dynamic stability derivatives for the condition of zero longitudinal acceleration at an angle of attack of 0° for each value of i_w . Constant power input to the model was maintained as angle of attack was changed during each test. The effect of thrust condition (simulating accelerated and decelerated flight conditions) on the dynamic stability derivatives was determined by conducting similar tests at different tunnel airspeeds with the same constant power input.

RESULTS AND DISCUSSION

The longitudinal stability characteristics measured in the investigation are discussed individually as static stability characteristics, in-phase oscillatory derivatives, and out-of-phase oscillatory derivatives. Longitudinal static stability characteristics measured in the investigation for wing incidence angles of 90° , 65° , 50° , 25° , 10° , and 0° are presented

in figures 8 to 13. The in-phase oscillatory derivatives are presented in figures 14 to 18 and are compared with the static data in figures 19 to 22. The out-of-phase oscillatory derivatives are presented in figures 23 to 27. In addition, scaled-up values of the model stability characteristics are presented in figures 28 and 29 for a hypothetical full-scale airplane for trimmed level flight throughout the forward speed range from hovering to conventional forward flight. Presented in table II are average values of the repeatability obtained during measurement of the oscillatory derivatives.

Static Stability Characteristics

The data of figure 8 show that, for the model in the hovering configuration, forward velocity produced positive pitching moments. This speed stability, although statically stabilizing, is primarily responsible for the controls-fixed unstable oscillation which occurred during the free-flight tests of reference 1. (A mathematical treatment of the importance of speed stability on handling qualities during hovering flight is given in ref. 3.) The data also indicated no appreciable variation of vertical force F_Z with forward speed. This aerodynamic characteristic, as pointed out in reference 3, leads to uncoupling of the vertical degree of freedom from the horizontal and angular degrees of freedom and makes the longitudinal oscillation essentially a two-degree-of-freedom oscillation involving horizontal displacement and pitching motion.

For the transition conditions, the variations of forces and moments presented in figures 9 to 12 show a progressive variation of the static longitudinal stability with wing incidence for angles of attack from about 0° to 10° , the range of greatest interest. For wing incidences of 65° and 50° the model was statically unstable with respect to angle of attack (positive M_{Y_α}) and was statically stable with respect to speed (positive M_{Y_V}). At a wing incidence angle of 25° , the model pitching-moment characteristics were extremely nonlinear with respect to angle of attack, although they generally indicated static instability in the angle-of-attack range from 0° to 10° . In addition, the speed stability derivative M_{Y_V} is positive for low speeds and negative for high speeds, although in the angle-of-attack range of 0° to 10° it is in all cases negative for small variations in velocity about trimmed level flight. For a wing incidence of 10° , the model was statically stable with respect to angle of attack and had negative speed stability (negative values of M_{Y_V}). The foregoing stability trends are in agreement with the flight test results of reference 1 where the stick-fixed dynamic stability of the model was observed to change from unstable oscillations for high wing incidence angles to stable motions at low angles. Presented in figure 13 are the variations with angle of attack of the conventional force and moment coefficients for the model with a wing incidence of 0° and propellers windmilling. These data are presented primarily as an aid in the interpretation of the damping data to be presented in a later section of this report.

In-Phase Oscillatory Derivatives

The variation of the in-phase oscillatory derivatives presented in figures 14 to 18 indicates that the model, in general, had positive values of the static stability parameter $M_{Y\alpha} - \omega^2 M_{Y\dot{q}}$ for wing incidence angles of 25° and above. This result is the same as that shown by the static data of figures 19 to 22. Values of the static stability parameters for unaccelerated level flight at an angle of attack of 0° as obtained from the static data of figures 9 to 13 and the oscillatory tests of figures 14 to 18 are compared in figures 19 to 22. The comparisons are generally good, but noticeable differences are present for some conditions. For example, in figures 21 and 22 at angles of attack between about 10° and 25° , there are large differences between the static and oscillation data. The wing is generally stalled in these conditions, and the differences are believed to be caused by the lag in buildup of the stalled flow conditions during the oscillation tests.

Out-of-Phase Derivatives

The variation of the out-of-phase oscillatory derivatives presented in figures 23 to 27 indicates that thrust conditions had significant effects on the out-of-phase oscillatory derivatives. At first glance, the unsystematic variation of the derivatives with thrust condition implies a great deal of scatter in the measured data but a study of table II indicates reasonable repeatability. The large effects of thrust condition on the damping derivatives probably result from extreme changes in the flow patterns about the model. The model had positive damping in pitch (negative values of $M_{Y\dot{q}} + M_{Y\ddot{\alpha}}$) for all conditions investigated. The magnitude of the damping in pitch increases as the wing incidence angle is decreased, as might be expected. The conventional damping-in-pitch parameter $C_{m\dot{q}} + C_{m\ddot{\alpha}}$ is approximately independent of angle of attack for a wing incidence of 0° with the propellers windmilling.

Stability Characteristics During Transition

The results of the investigation for trimmed level flight at an angle of attack of 0° are summarized by the data of figures 28 and 29 which present the longitudinal stability characteristics of a full-scale airplane as functions of forward velocity from hovering to conventional forward flight. These data were obtained by scaling up the model data. The dimensional damping-in-pitch model data were scaled up by multiplying by the fourth power of the model scale factor (9^4) and by the ratio of full-scale speed to model speed. The full-scale airplane was assumed to have a wing loading of 70 pounds per square foot (3352 N/m^2) and a moment of inertia in pitch I_y of 125 000 slug-ft² ($169\,476 \text{ kg-m}^2$) on the basis of data presented in reference 1.

The unbalanced pitching moment which would have to be trimmed by the tail rotor or horizontal tail (a different tail incidence program being used) is presented as a

function of velocity in figure 28. The pitching-moment values are positive for velocities below about 28 knots and negative for speeds above this point. The variation of the static stability parameter $M_{Y\alpha} - \omega^2 M_{Y\dot{q}}$ presented in figure 29 shows the airplane to be statically unstable with respect to angle of attack for speeds below about 70 knots which correspond to wing incidence angles above about 15° . Variation of the damping-in-pitch parameter $M_{Y\dot{q}} + M_{Y\dot{\alpha}}$ shows that the damping in pitch of the airplane increases as forward speed increases and as the horizontal tail becomes more effective.

CONCLUSIONS

An investigation of the static and dynamic longitudinal stability derivatives of a 1/9-scale model of a four-propeller tilt-wing V/STOL transport aircraft indicates the following conclusions:

1. The model was statically unstable with respect to angle of attack for level flight with zero longitudinal acceleration for wing incidence angles above about 15° and was stable for angles below this value.

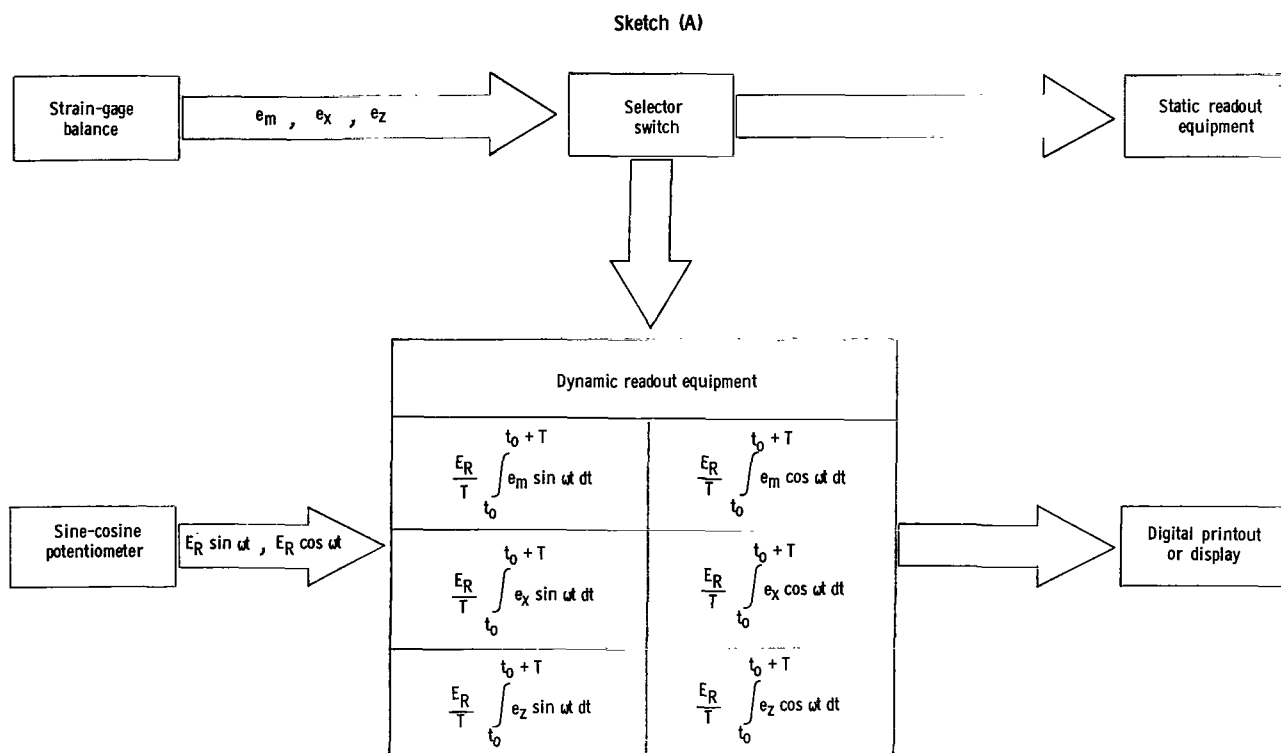
2. The model had positive damping in pitch (negative values of the damping-in-pitch parameter $M_{Y\dot{q}} + M_{Y\dot{\alpha}}$) for all wing incidence angles, thrust conditions, and angles of attack investigated.

Langley Research Center,
National Aeronautics and Space Administration,
Langley Station, Hampton, Va., May 17, 1966.

APPENDIX A

INSTRUMENTATION AND DATA REDUCTION

The present investigation utilized a six-channel return signal analyzer to obtain the dynamic oscillatory derivatives. This equipment resulted in extremely rapid data acquisition in comparison with previous methods. A block diagram of the data reduction system is shown in sketch (a).



The output of one strain-gage element, for example, the pitching moment, can be expressed as

$$e_m = M_Y k_m E \quad (A1)$$

This voltage signal is returned to two of the signal analyzer channels. In one channel, the pitching-moment signal is multiplied by the in-phase voltage return signal of the sine-cosine potentiometer ($E_R \sin \omega t$) whereas in the second channel the moment voltage is multiplied by the out-of-phase signal ($E_R \cos \omega t$). The resulting voltages for the multiplications are

APPENDIX A

$$\text{In-phase voltage} = E_{\text{in}} = e_m E_R \sin \omega t \quad (\text{A2})$$

$$\text{Out-of-phase voltage} = E_{\text{out}} = e_m E_R \cos \omega t \quad (\text{A3})$$

If small perturbation analysis is assumed to apply, the total aerodynamic pitching moment M_Y can be expressed as

$$M_Y = M_{Y_0} + M_{Y_\alpha} \Delta\alpha + M_{Y_{\dot{\alpha}}} \Delta\dot{\alpha} + M_{Y_q} \Delta q + M_{Y_{\dot{q}}} \Delta\dot{q} \quad (\text{A4})$$

Also, the oscillatory motions generated by the oscillatory equipment produce the following kinematical relations:

$$\left. \begin{aligned} \Delta\alpha &= \Delta\alpha_{\text{max}} \sin \omega t & \Delta\dot{\theta} &= \omega \Delta\theta_{\text{max}} \cos \omega t = \Delta q \\ \Delta\dot{\alpha} &= \omega \Delta\alpha_{\text{max}} \cos \omega t & \Delta\ddot{\theta} &= -\omega^2 \Delta\theta_{\text{max}} \sin \omega t = \Delta\dot{q} \\ \Delta\theta_{\text{max}} &= \Delta\alpha_{\text{max}} \end{aligned} \right\} \quad (\text{A5})$$

Substituting relations (A5), equation (A1), and equation (A4) into equations (A2) and (A3) yields (only the in-phase result is shown for convenience)

$$E_{\text{in}} = E_R k_m E \sin \omega t \left[M_{Y_0} + \left(M_{Y_\alpha} - \omega^2 M_{Y_{\dot{q}}} \right) \Delta\alpha_{\text{max}} \sin \omega t + \left(M_{Y_q} + M_{Y_{\dot{\alpha}}} \right) \omega \Delta\alpha_{\text{max}} \cos \omega t \right] \quad (\text{A6})$$

The in-phase analyzer channel finds the average value of this voltage as

$$\bar{E}_{\text{in}} = \frac{1}{T} \int_{t_0}^{t_0+T} E_{\text{in}} dt \quad (\text{A7})$$

Substituting equation (A6) into equation (A7) and integrating yields

$$\bar{E}_{\text{in}} = \frac{K_m \Delta\alpha_{\text{max}}}{2} \left(M_{Y_\alpha} - \omega^2 M_{Y_{\dot{q}}} \right)$$

for which

$$M_{Y_\alpha} - \omega^2 M_{Y_{\dot{q}}} = \frac{2\bar{E}_{\text{in}}}{K_m \Delta\alpha_{\text{max}}} \quad (\text{A8})$$

where $K_m = E_R k_m E$.

APPENDIX A

The out-of-phase derivative is obtained from the second analyzer channel. The equation obtained is

$$M_{Y_q} + M_{Y_{\dot{\alpha}}} = \frac{2\bar{E}_{out}}{K_m \omega \Delta \alpha_{max}} \quad (A9)$$

Equations (A8) and (A9) can be nondimensionalized to obtain standard nondimensional derivative combinations:

$$C_{m_q} + C_{m_{\dot{\alpha}}} = \frac{2V}{q_{\infty} S \bar{c}^2} (M_{Y_q} + M_{Y_{\dot{\alpha}}})$$

$$C_{m_{\alpha}} - \left(\frac{\omega \bar{c}}{2V}\right)^2 C_{m_{\dot{q}}} = \frac{1}{q_{\infty} S \bar{c}} (M_{Y_{\alpha}} - \omega^2 M_{Y_{\dot{q}}})$$

The voltage values of interest (E_{in} and E_{out}) are stored in the response analyzer channels. A single pushbutton operation begins a sequential scanning process in which the data of each channel may be either displayed on a digital voltmeter and/or printed on paper tape for further data analysis.

REFERENCES

1. Newsom, William A., Jr.; and Kirby, Robert H.: Flight Investigation of Stability and Control Characteristics of a 1/9-Scale Model of a Four-Propeller Tilt-Wing V/STOL Transport. NASA TN D-2443, 1964.
2. Mechtly, E. A.: The International System of Units – Physical Constants and Conversion Factors. NASA SP-7012, 1964.
3. Seckel, Edward: Stability and Control of Airplanes and Helicopters. Academic Press, Inc., c.1964.
4. Deckert, Wallace H.; Page, V. Robert; and Dickinson, Stanley O.: Large-Scale Wind-Tunnel Tests of Descent Performance of an Airplane Model With a Tilt Wing and Differential Propeller Thrust. NASA TN D-1857, 1964.

TABLE I.- GEOMETRIC CHARACTERISTICS OF THE MODEL

Fuselage:

Length, ft (m)	5.56 (1.69)
Cross-sectional area, maximum, sq ft (sq m)	1.01 (0.09)
Height, maximum, ft (m)	1.36 (0.41)
Width, maximum, ft (m)	1.01 (0.31)

Wing:

Area, sq ft (sq m)	6.60 (0.61)
Span, ft (m)	7.50 (2.29)
Aspect ratio	8.53
Mean aerodynamic chord, ft (m)	0.90 (0.27)
Airfoil section	NACA 633-318
Tip chord, ft (m)	0.67 (0.20)
Root chord, ft (m)	1.09 (0.33)
Taper ratio	0.61
Sweepback of quarter chord, deg	4.13
Dihedral angle, deg	-2.12
Pivot station, percent root chord	42.5

Aileron, each:

Chord, percent wing chord	25
Area, sq ft (sq m)	0.38 (0.03)

Flap, each:

Type	Double slotted
Chord, percent wing chord	47
Span	Full

Slat, each:

Inboard, 0.45 wing semispan to	
0.69 wing semispan	Chord, 0.20 wing chord inboard to 0.10 wing chord outboard
Outboard, 0.85 wing semispan to	
1.00 wing semispan	Chord, 0.10 wing chord full length

Vertical tail:

Area, sq ft (sq m)	1.61 (0.15)
Span, ft (m)	1.73 (0.53)
Aspect ratio	1.87

TABLE I.- GEOMETRIC CHARACTERISTICS OF THE MODEL - Concluded

Airfoil section:		
Root		NACA 0018
Tip		NACA 0012
Tip chord, ft (m)	0.37	(0.11)
Root chord, ft (m)	1.48	(0.45)
Taper ratio	0.25	
Sweepback of quarter chord, deg	26	
Rudder:		
Tip chord, ft (m)	0.15	(0.05)
Root chord, ft (m)	0.42	(0.13)
Span, measured from tip chord, ft (m)	1.06	(0.32)
Tail length, center of gravity to 0.25 mean aerodynamic		
chord, ft (m)	2.38	(0.73)
Horizontal tail:		
Area, sq ft (sq m)	2.11	(0.20)
Aspect ratio	5.68	
Airfoil section:		
Root		NACA 0015
Tip		NACA 0012
Tip chord, ft (m)	0.39	(0.12)
Root chord, ft (m)	0.78	(0.24)
Span, ft (m)	3.46	(1.05)
Taper ratio	0.50	
Sweepback of quarter chord, deg	9.50	
Mean aerodynamic chord, ft (m)	0.61	(0.19)
Tail length, center of gravity to 0.25 mean aerodynamic		
chord, ft (m)	2.76	(0.84)
Propellers:		
Main:		
Number of blades	4	
Diameter, ft (m)	1.72	(0.52)
Tail:		
Number of blades	3	
Diameter, ft (m)	0.89	(0.27)
Moment arm, wing pivot to rotor center, ft (m)	3.56	(1.09)

TABLE II. - REPEATABILITY OF OSCILLATORY DATA

[Values are indicative of maximum average deviation of oscillatory data]

Parameter	Wing incidence angle			
	10°	25°	50°	65°
$\frac{F_{X\alpha} - \omega^2 F_{X\dot{q}}}{L_0}$	±0.010	±0.013	±0.010	±0.008
$\frac{F_{Z\alpha} - \omega^2 F_{Z\dot{q}}}{L_0}$	±0.030	±0.025	±0.020	±0.018
$\frac{M_{Y\alpha} - \omega^2 M_{Y\dot{q}}}{L_0 \bar{c}}$	±0.050	±0.031	±0.008	±0.012
$F_{Xq} + F_{X\dot{\alpha}}$	±0.039	±0.100	±0.150	±0.130
$F_{Zq} + F_{Z\dot{\alpha}}$	±0.161	±0.250	±0.200	±0.200
$\frac{M_{Yq} + M_{Y\dot{\alpha}}}{\bar{c}}$	±0.140	±0.170	±0.120	±0.130

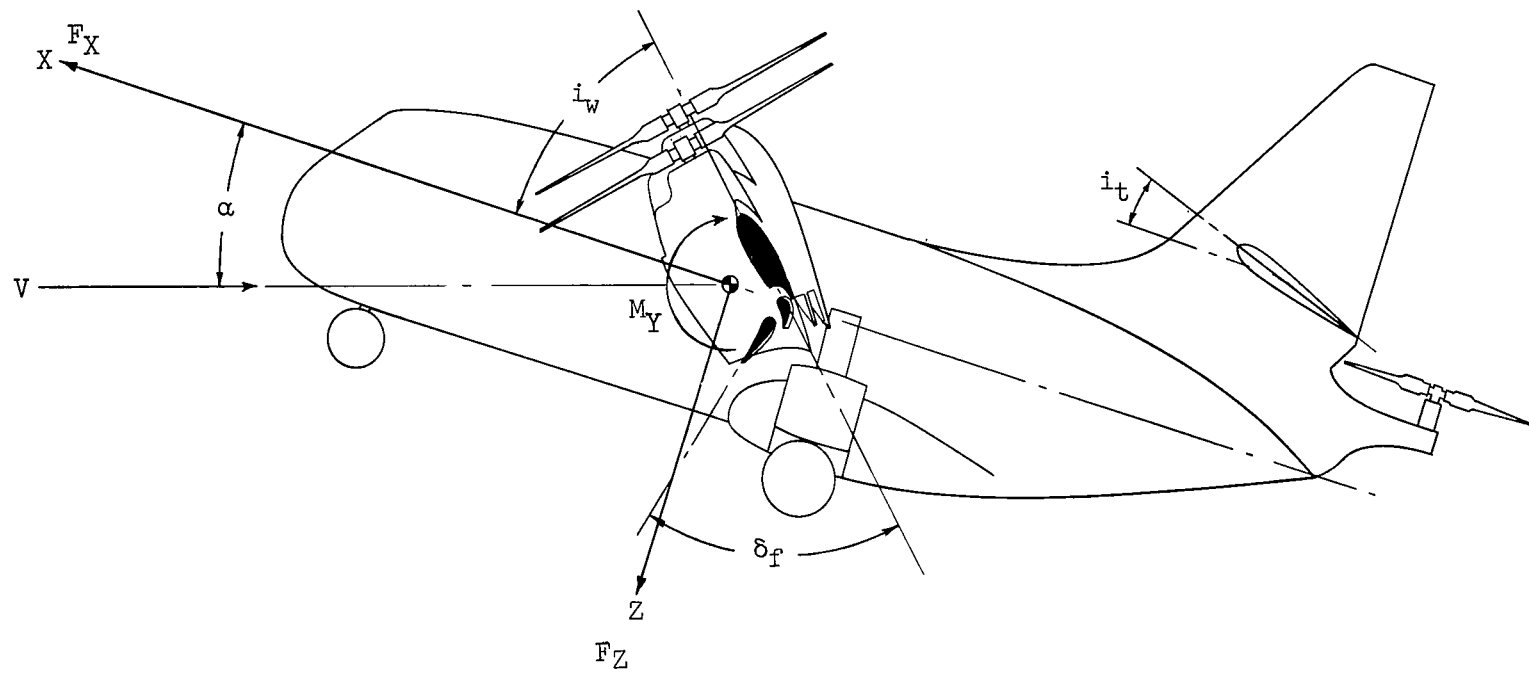


Figure 1.- Body system of axes. Positive senses of forces and moments are indicated.

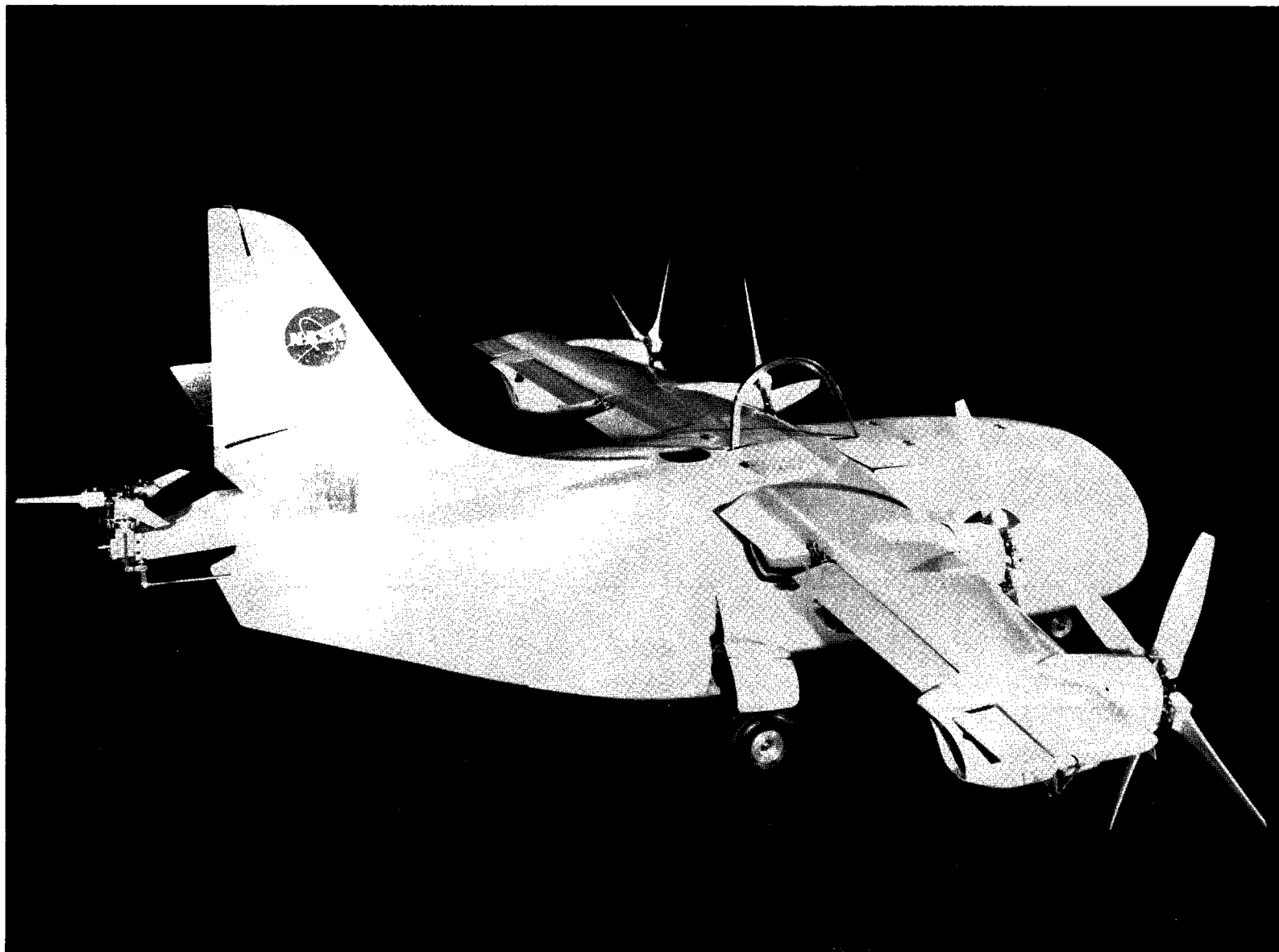


Figure 2.- Photograph of model.

L-62-6321

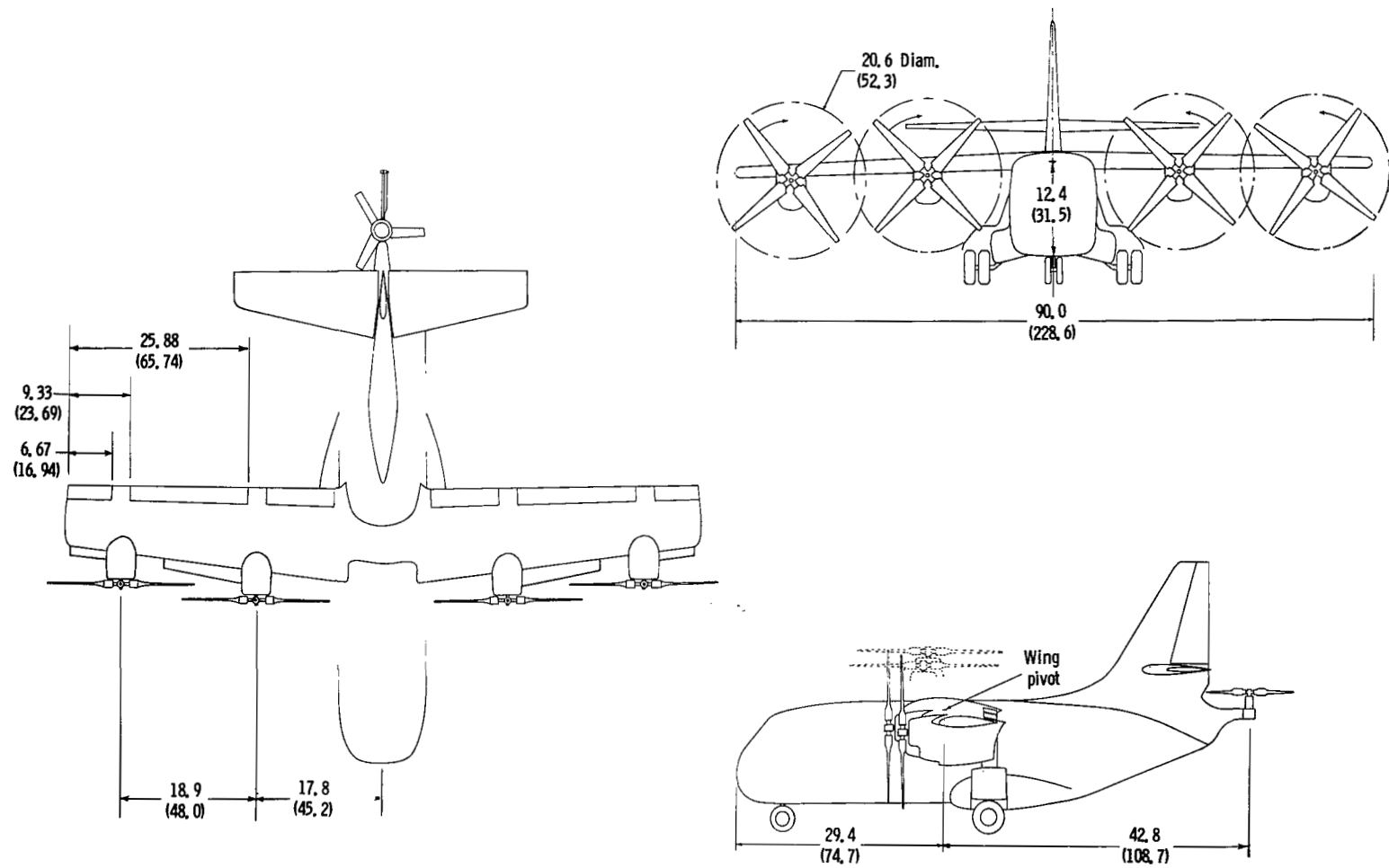


Figure 3.- Three-view sketch of model. Dimensions are given in inches and parenthetically in centimeters.

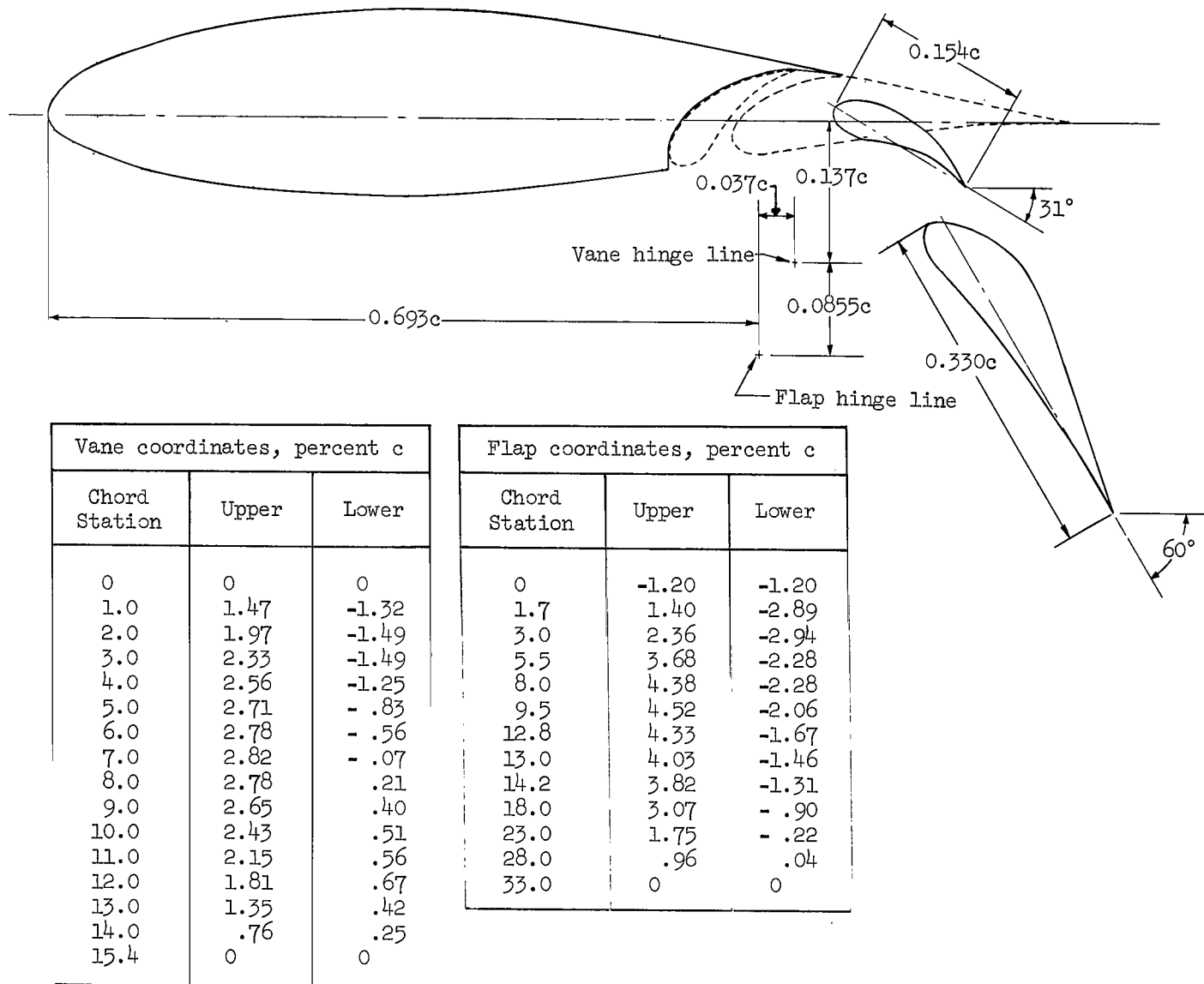


Figure 4.- Typical cross section of wing showing details of flap system.

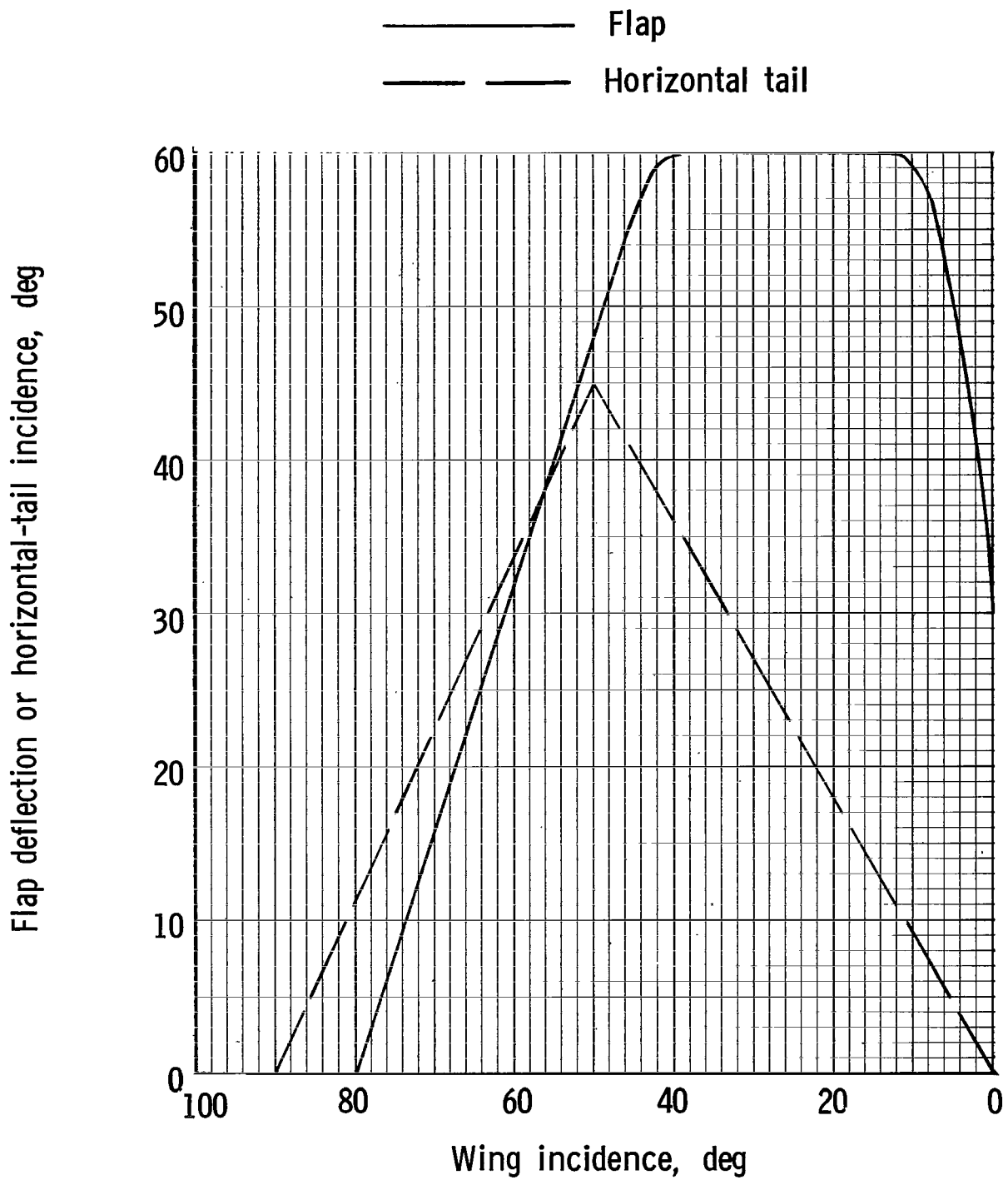


Figure 5.- Variation of flap deflection or horizontal-tail incidence with wing incidence.

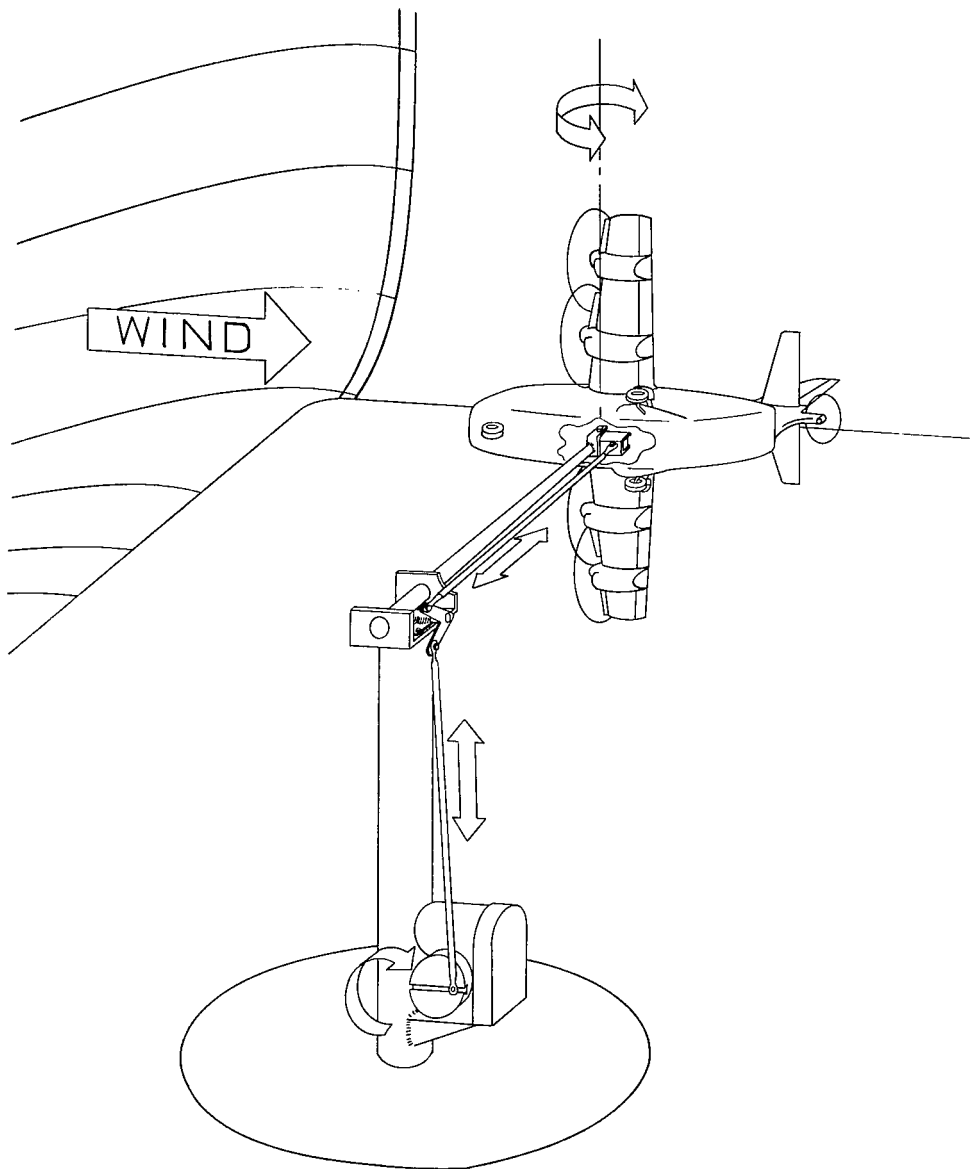


Figure 6.- Sketch of test setup for oscillatory force tests.

Distance of moment reference center
below wing pivot, percent \bar{c}

Distance of moment reference center
forward of wing pivot, percent \bar{c}

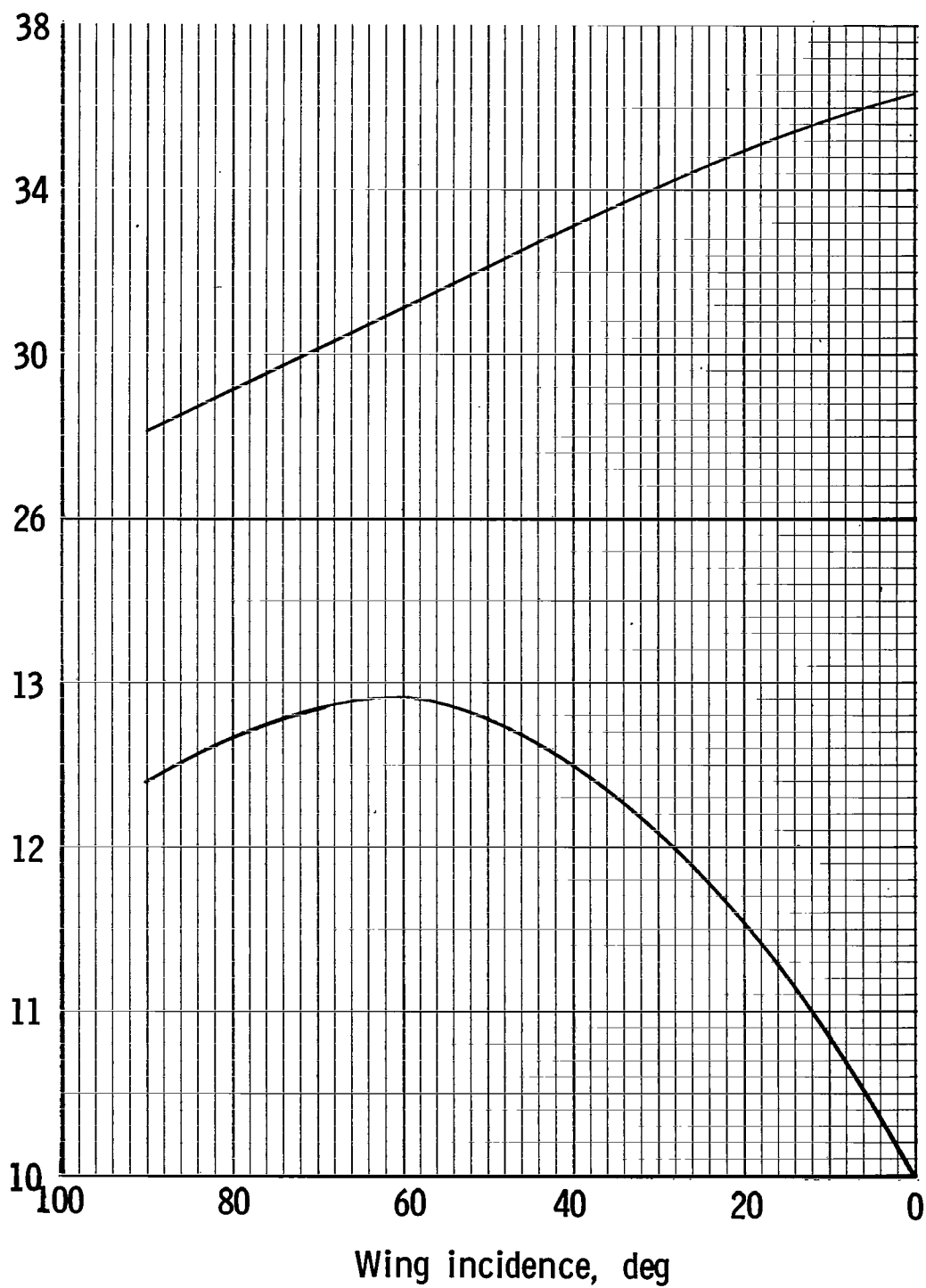


Figure 7.- Location of moment reference center as a function of wing incidence angle.

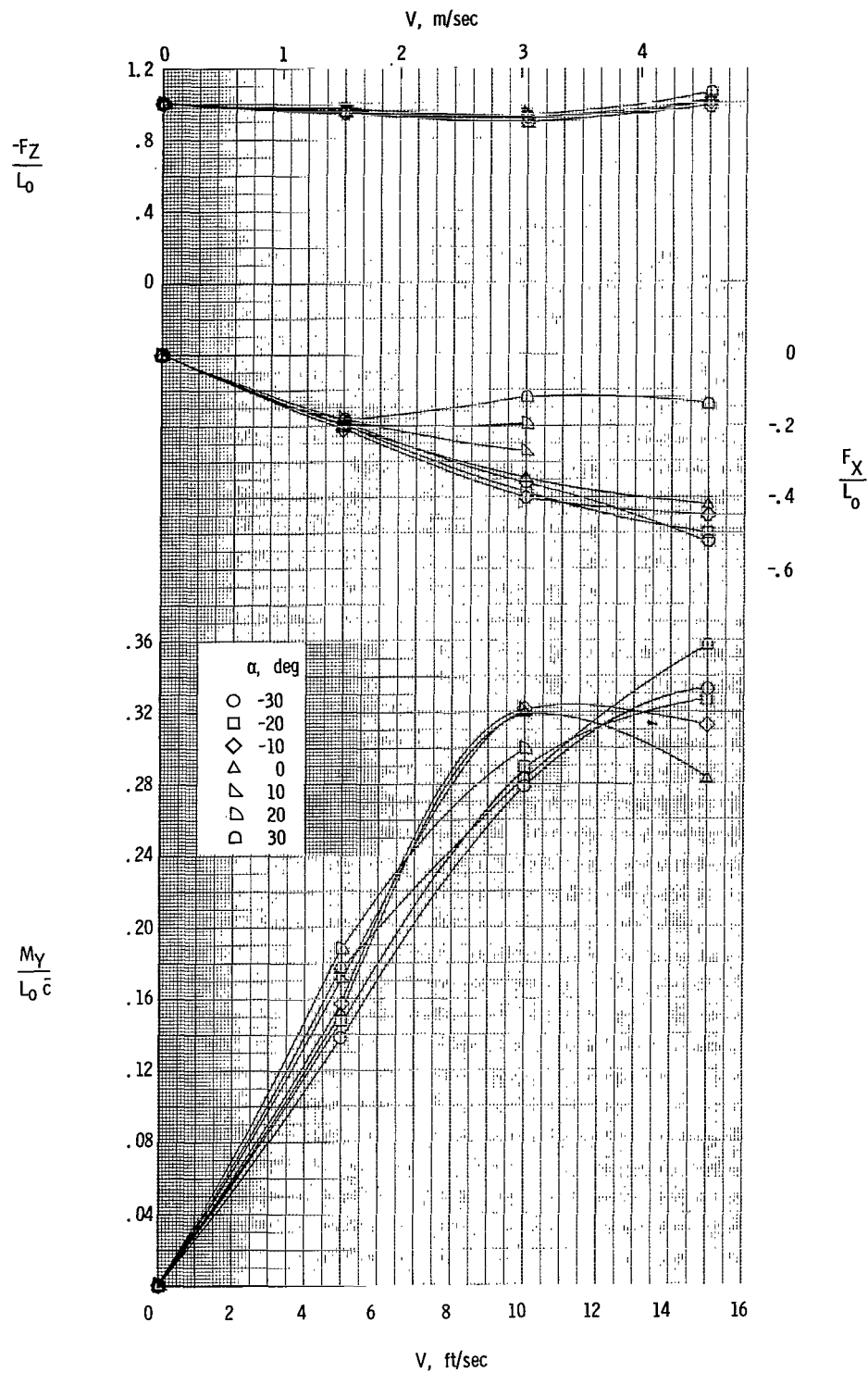


Figure 8.- Variation of forces and moments with velocity for hovering configuration. $i_w = 90^\circ$; $i_t = 0^\circ$; $L_0 = 31.65$ lb (140.79 N).

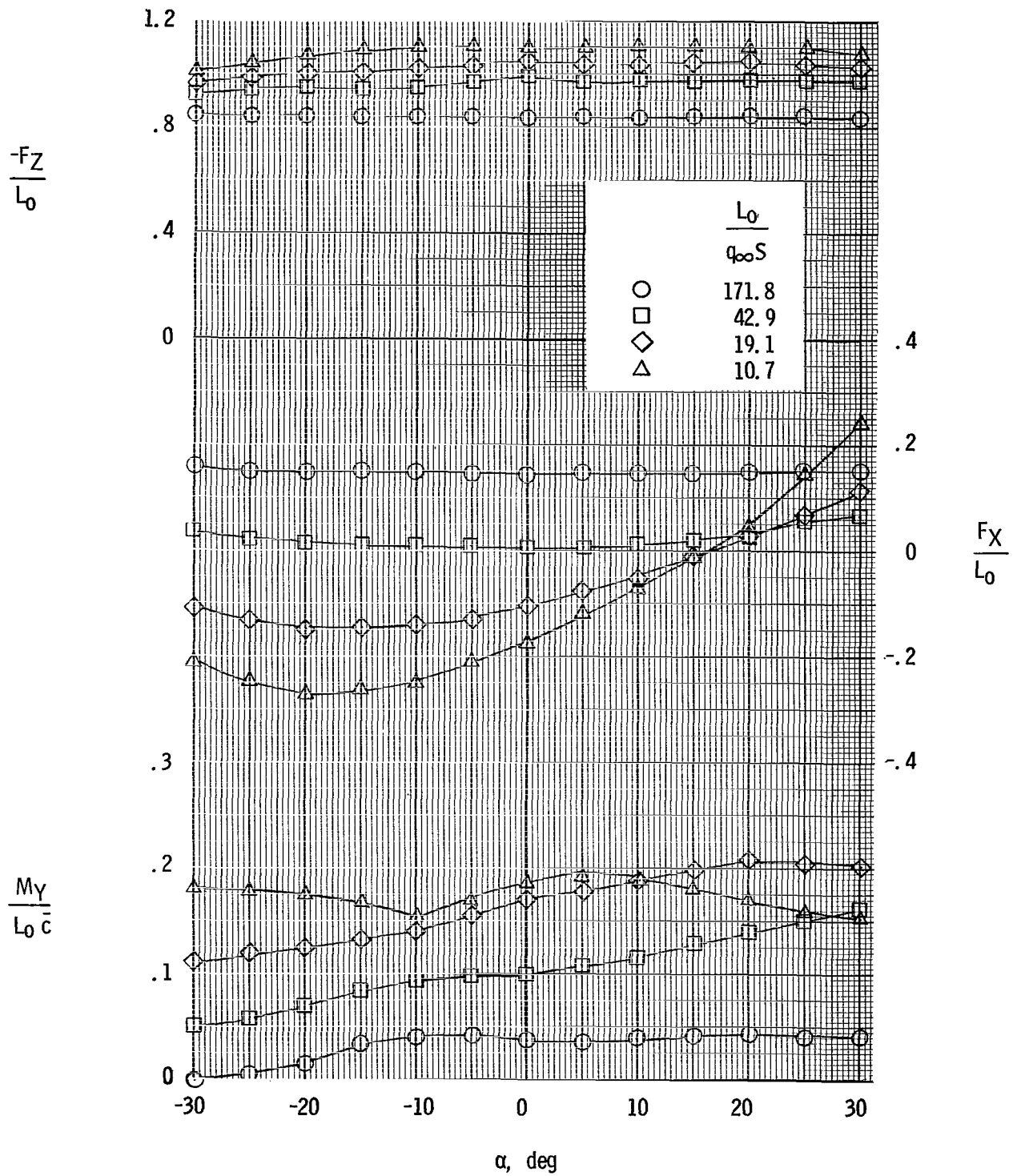


Figure 9.- Variation of static longitudinal characteristics with angle of attack. $i_w = 65^\circ$; $i_t = 28^\circ$.

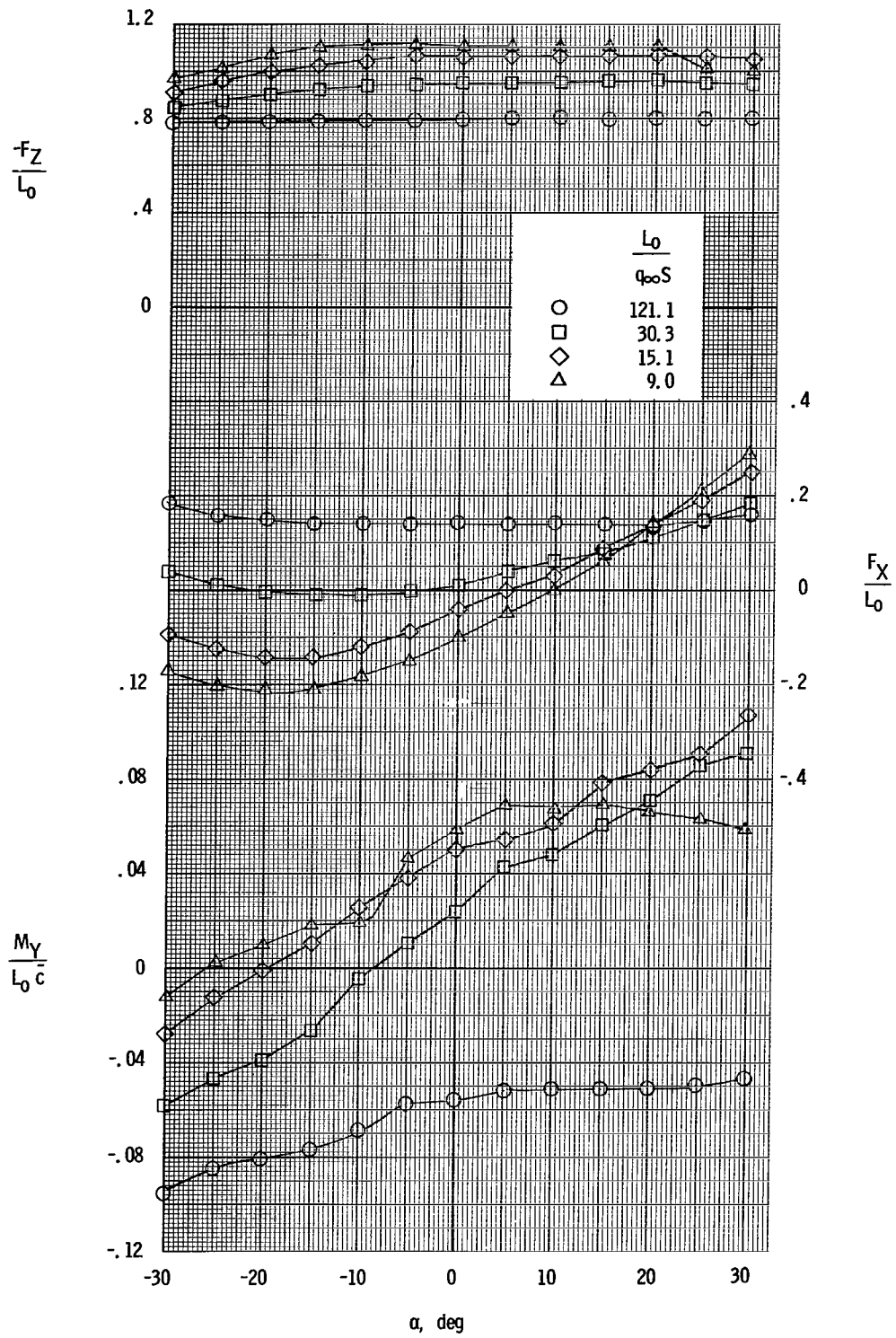


Figure 10.- Variation of static longitudinal characteristics with angle of attack. $i_w = 50^\circ$; $i_t = 45^\circ$.

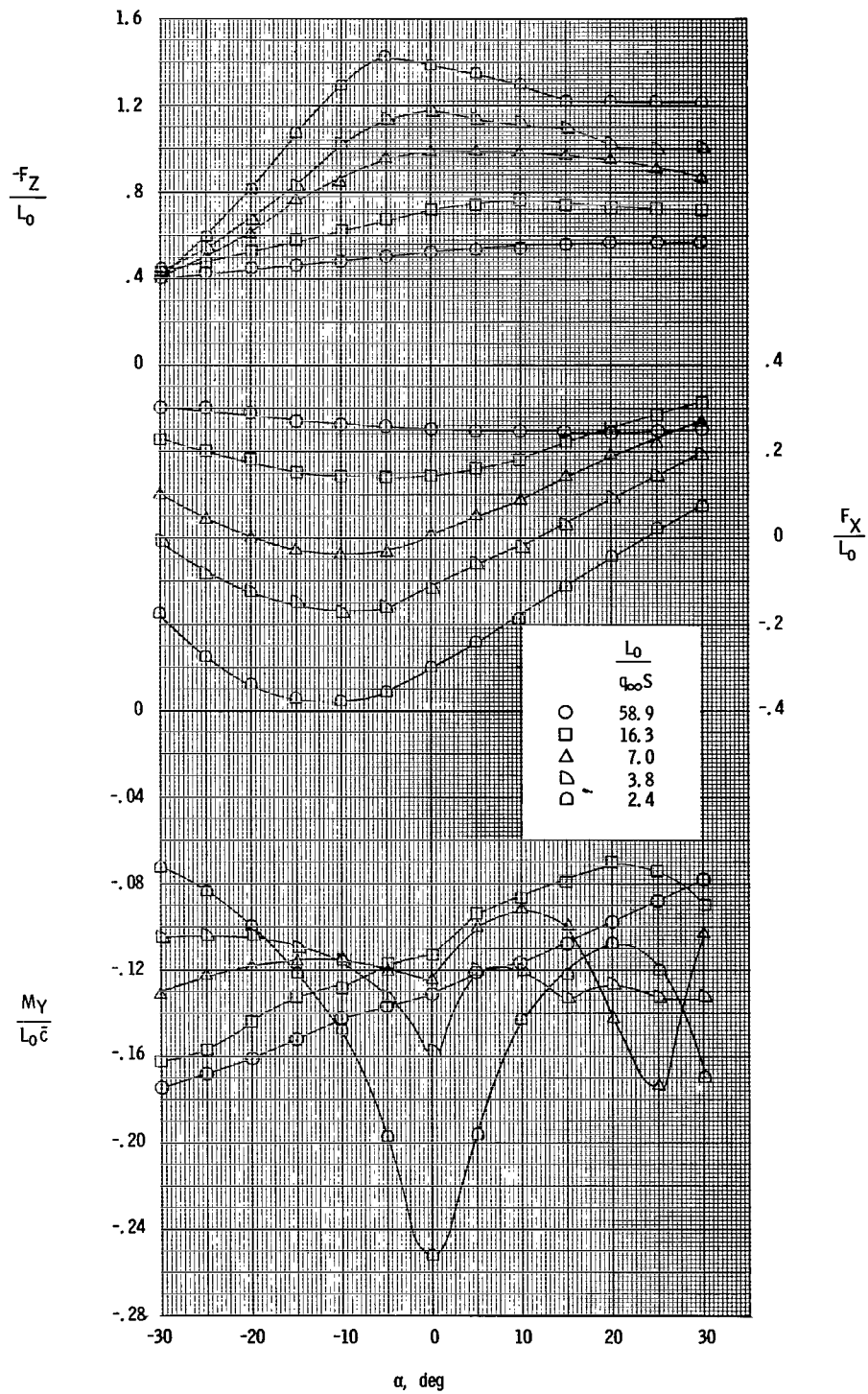


Figure 11.- Variation of static longitudinal characteristics with angle of attack. $i_w = 25^\circ$; $i_t = 23^\circ$.

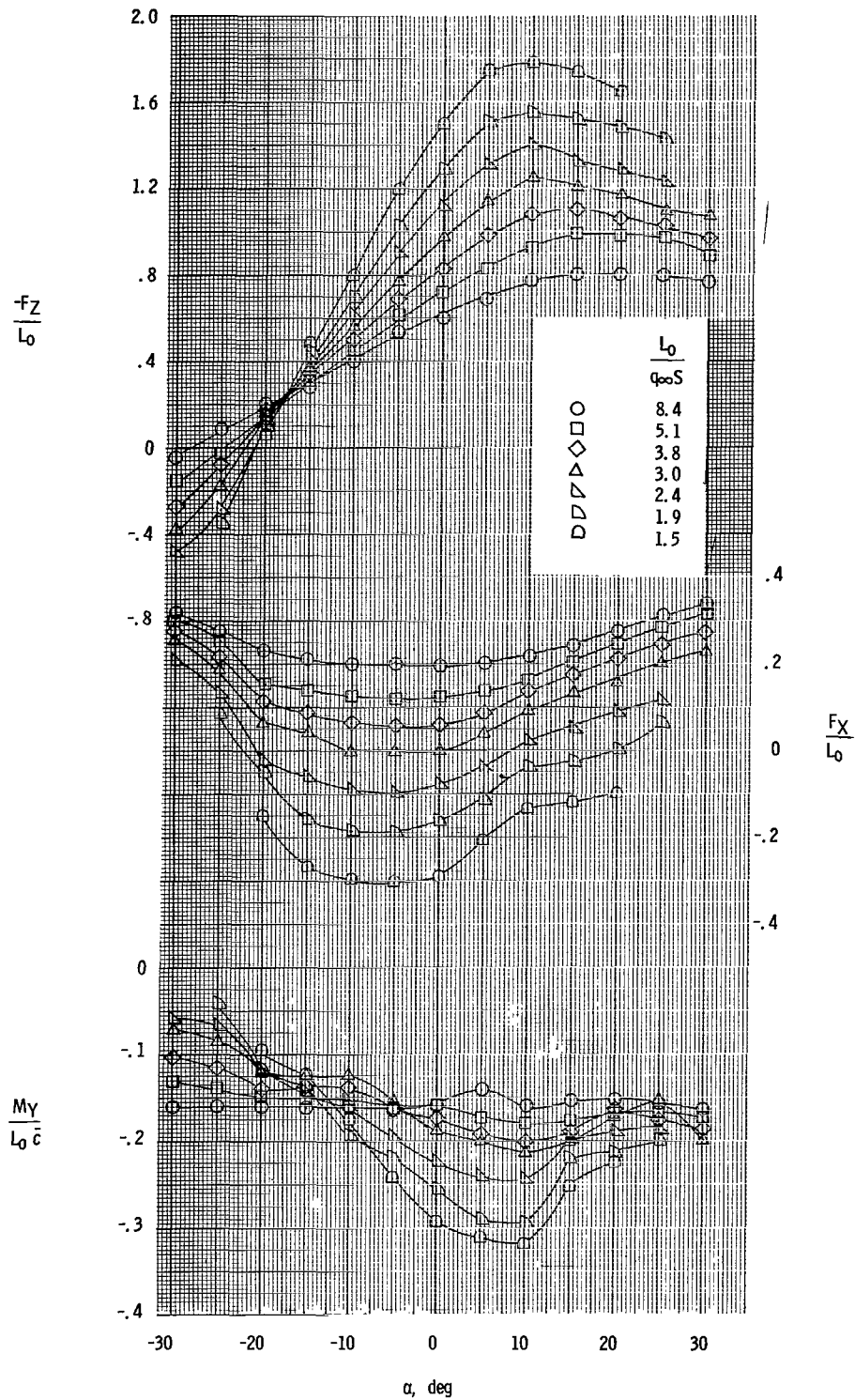


Figure 12.- Variation of static longitudinal characteristics with angle of attack. $i_w = 10^\circ$; $i_t = 10^\circ$.

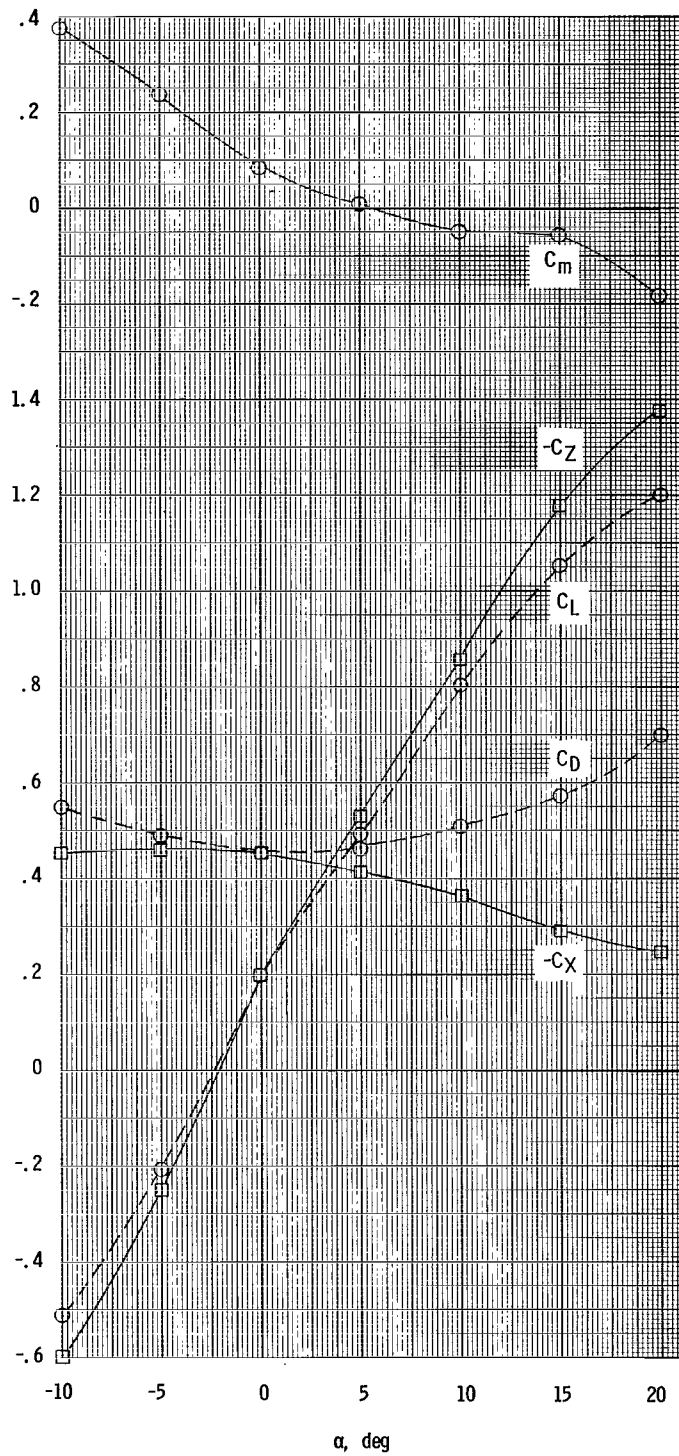


Figure 13.- Variation of static longitudinal characteristics with angle of attack. $i_w = 0^\circ$; $i_t = 0^\circ$; $\delta_f = 0^\circ$; propellers windmilling.

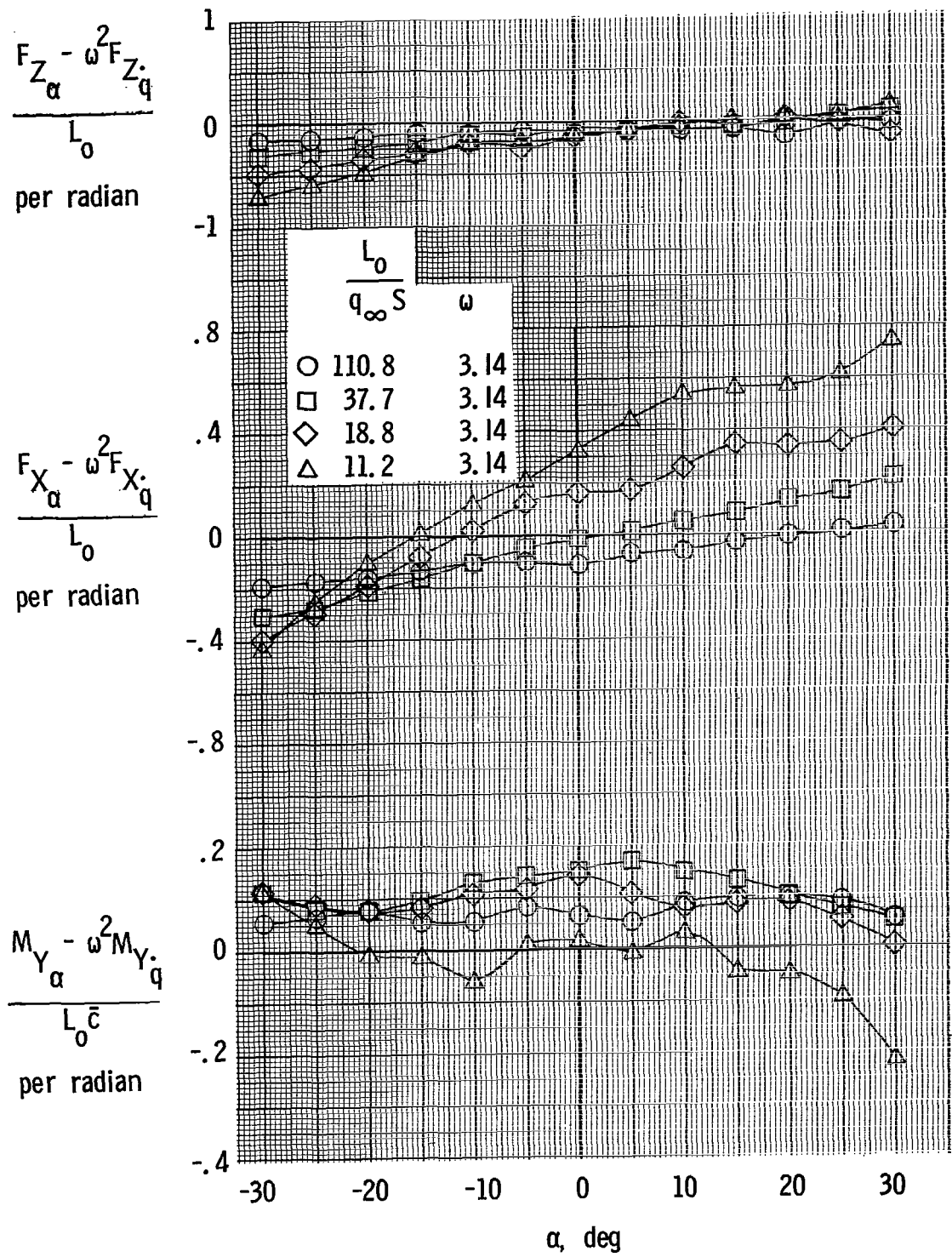


Figure 14.- Variation of in-phase oscillatory derivatives with angle of attack. $i_w = 65^\circ$; $i_t = 28^\circ$.

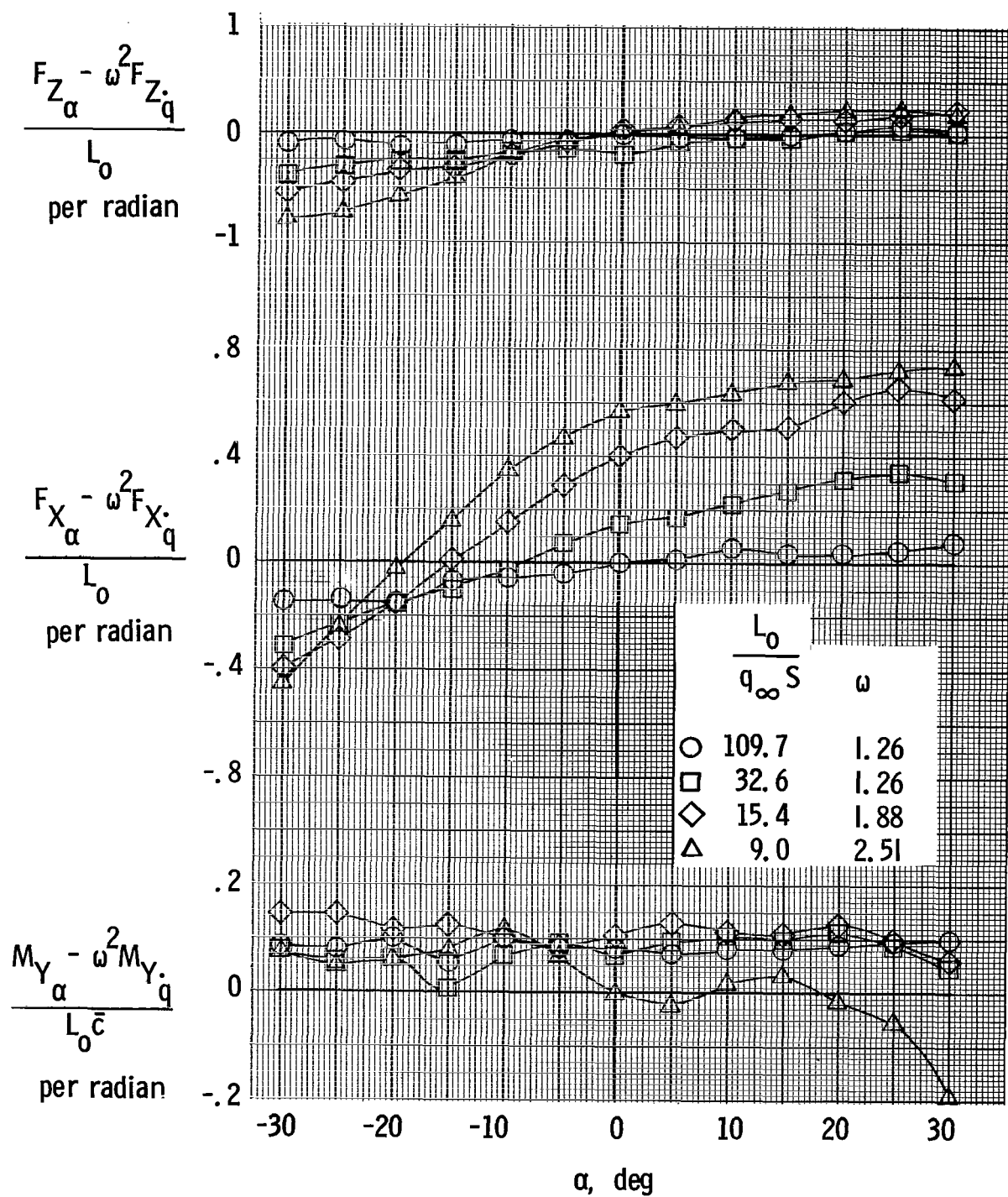


Figure 15.- Variation of in-phase oscillatory derivatives with angle of attack. $i_w = 50^\circ$; $i_t = 45^\circ$.

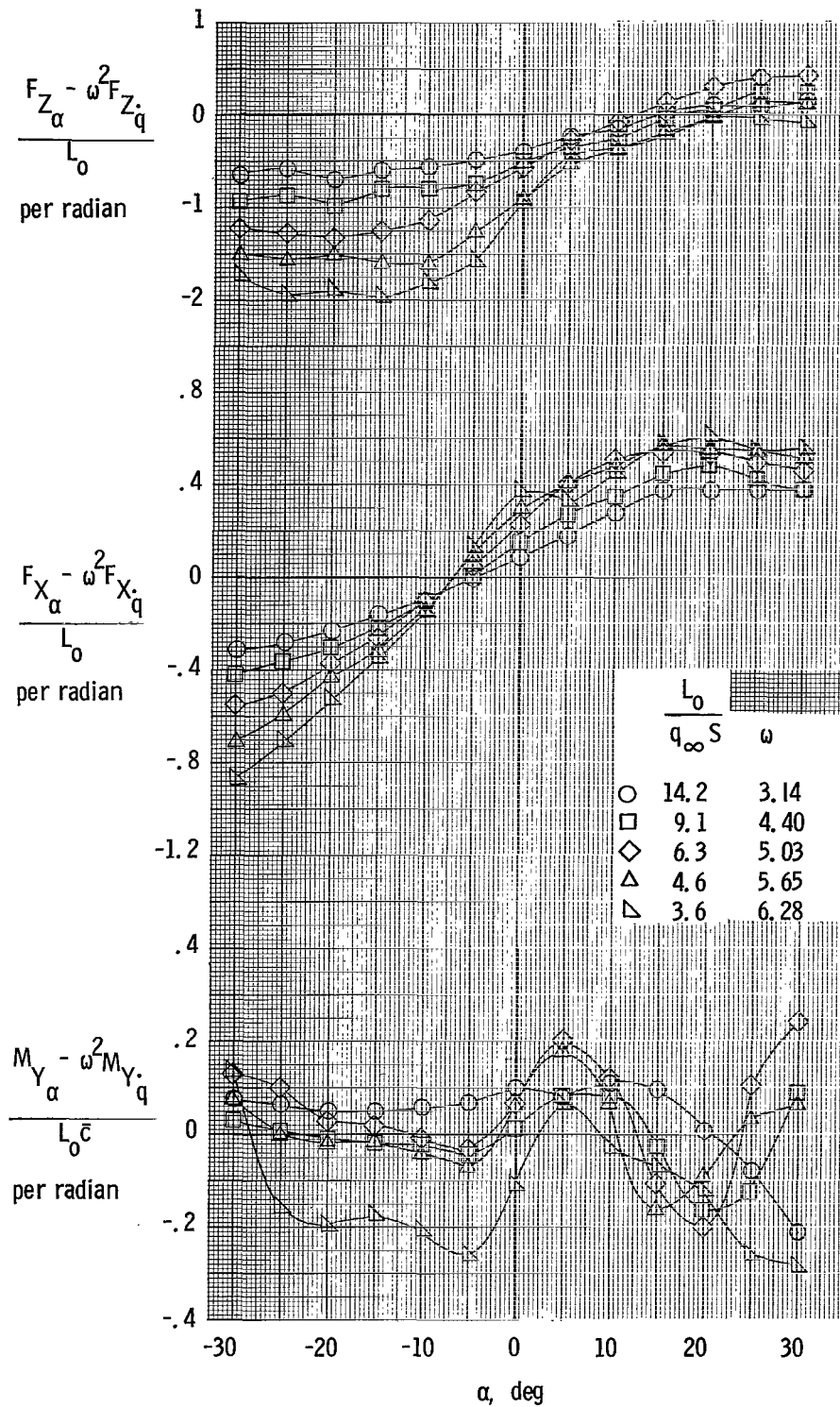


Figure 16.- Variation of in-phase oscillatory derivatives with angle of attack. $i_w = 25^\circ$; $i_t = 23^\circ$.

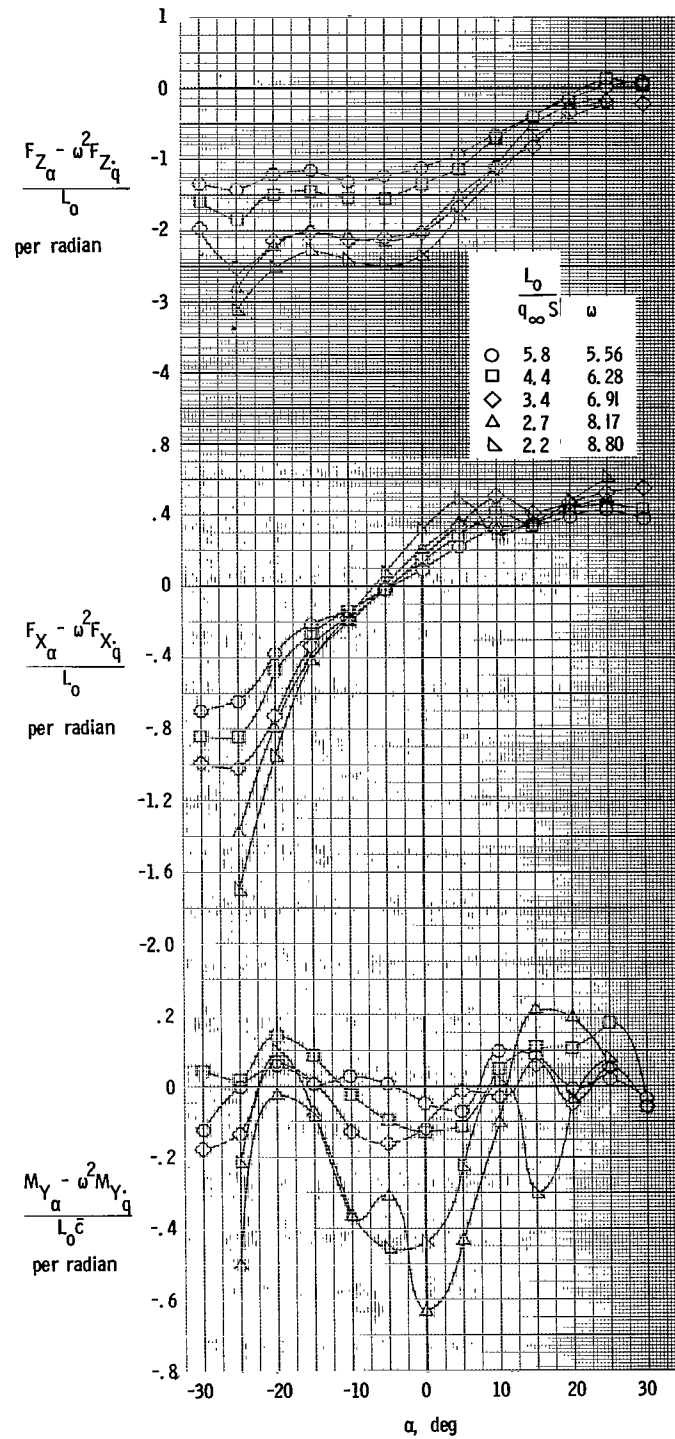


Figure 17.- Variation of in-phase oscillatory derivatives with angle of attack. $i_w = 10^\circ$; $i_t = 10^\circ$.

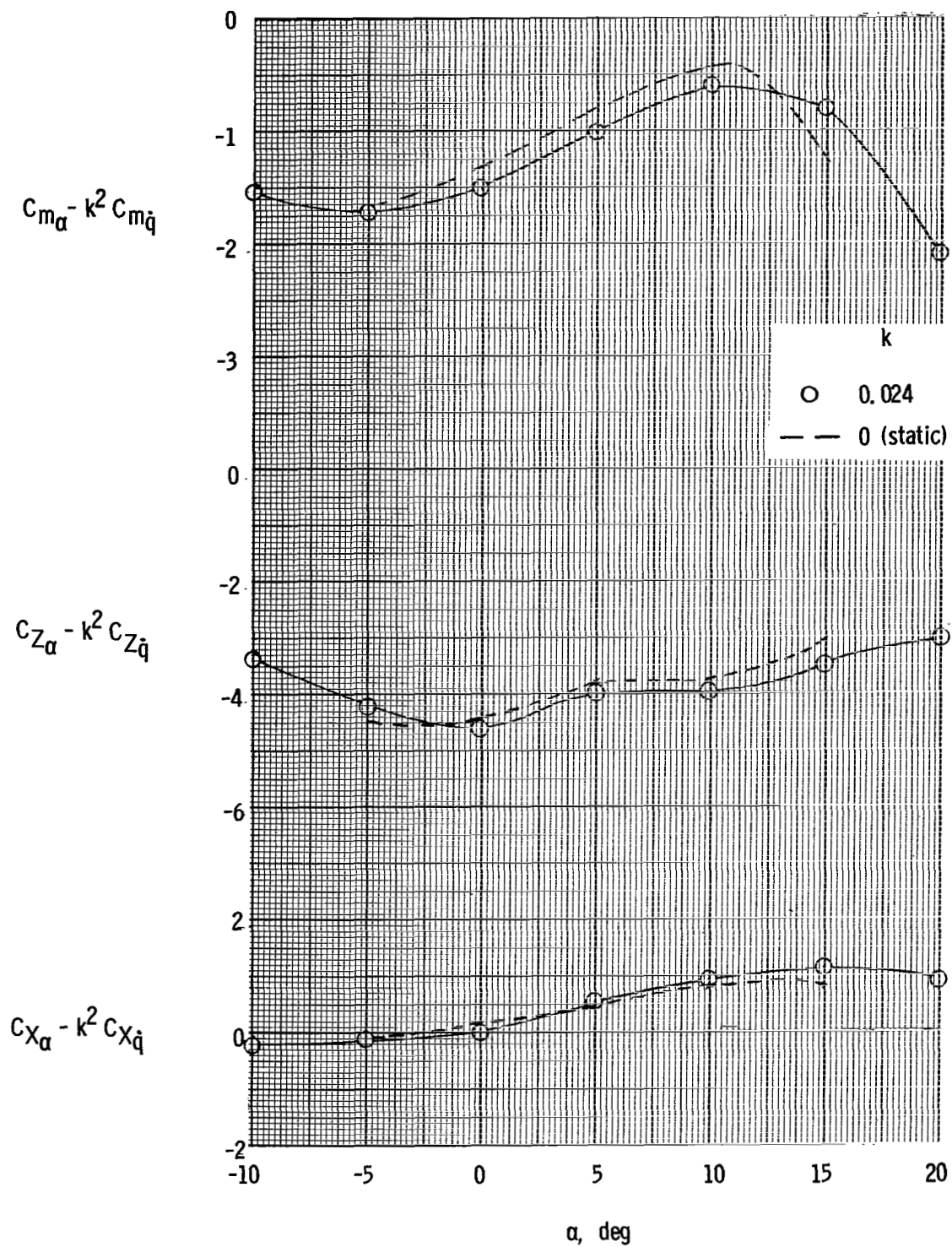


Figure 18.- Variation of in-phase oscillatory derivatives with angle of attack. $i_w = 0^\circ$; propellers windmilling.

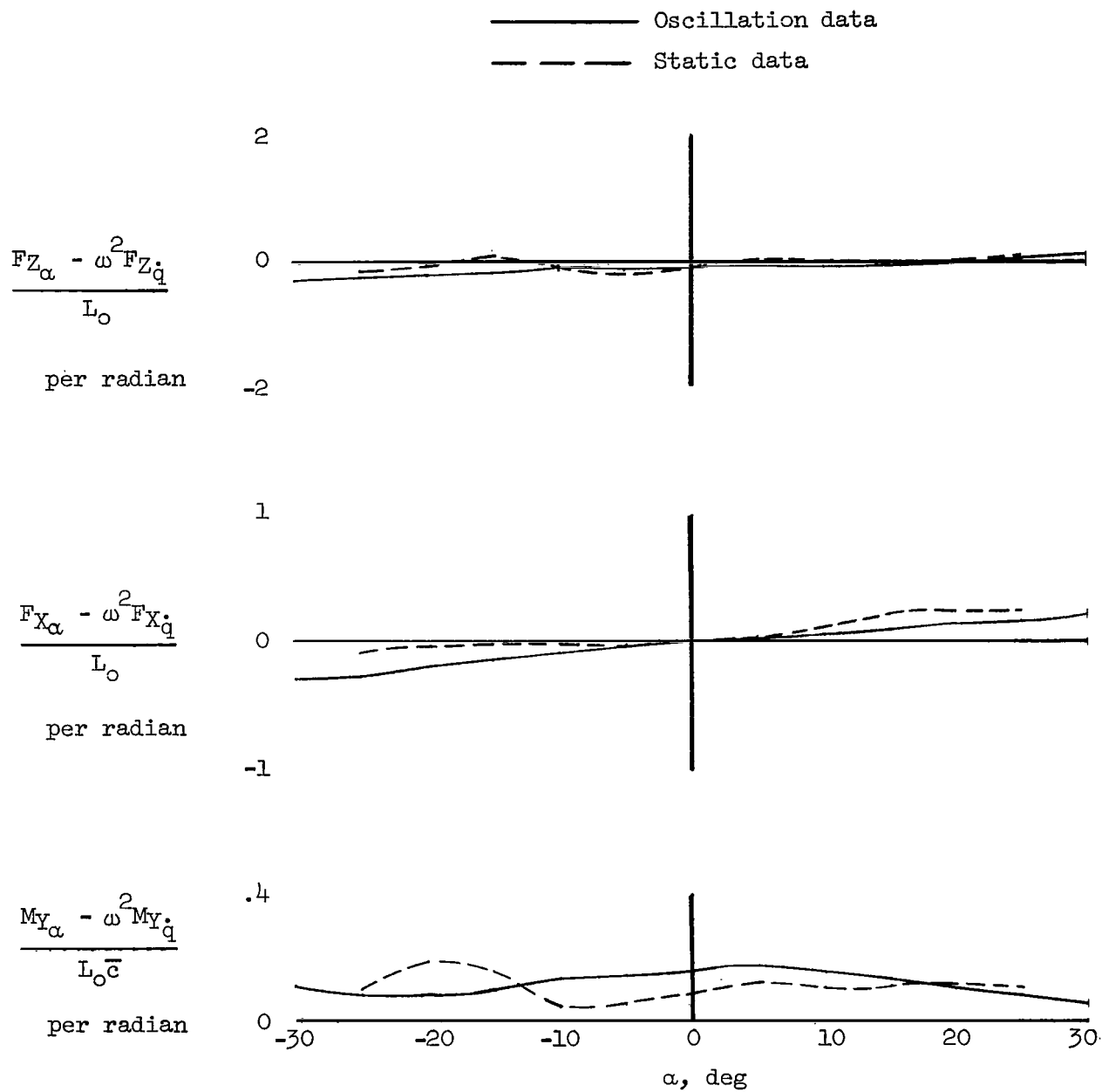


Figure 19.- Comparison of in-phase oscillatory and static data for $i_w = 65^\circ$.

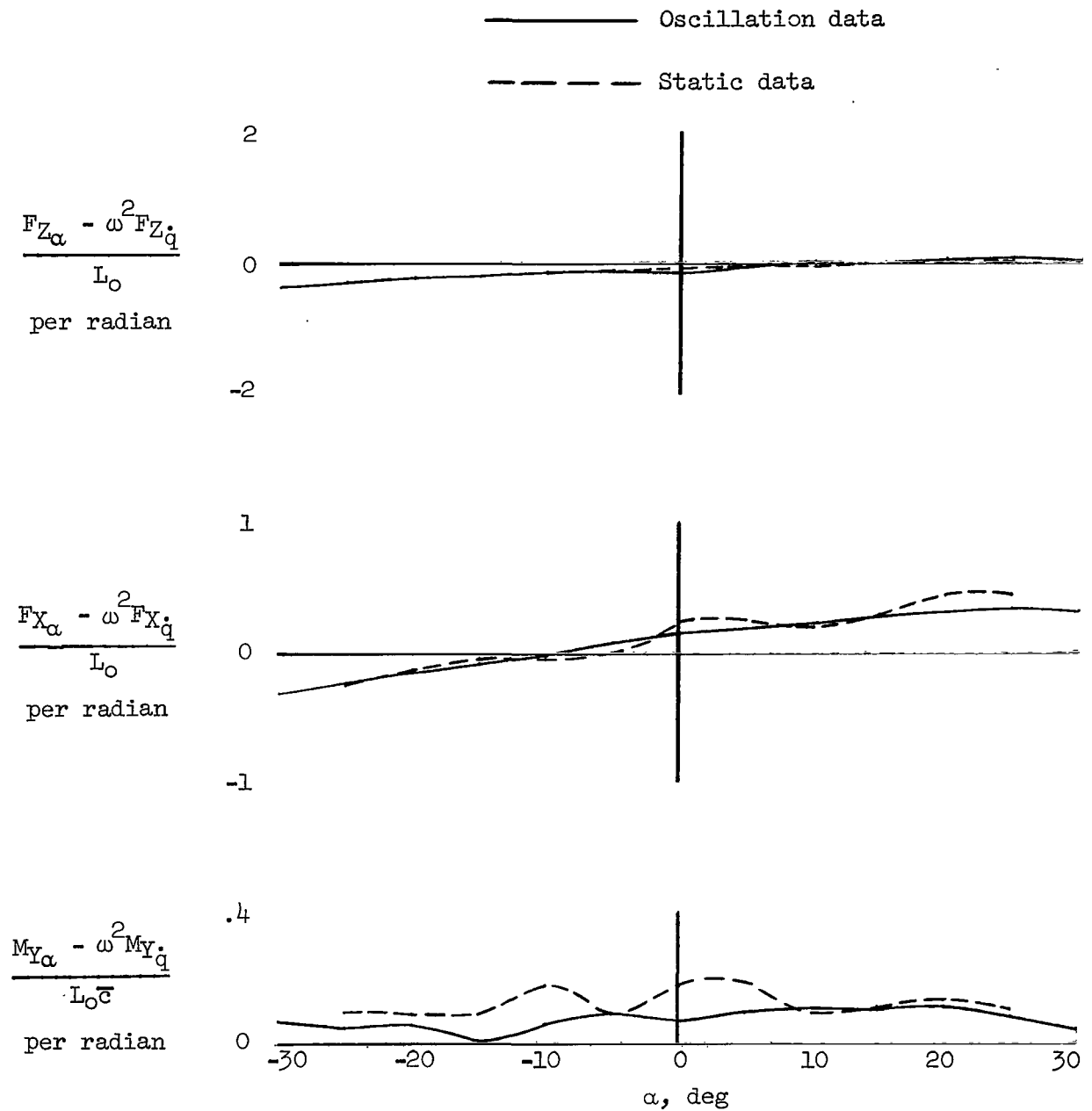


Figure 20.- Comparison of in-phase oscillatory and static data for $i_w = 50^\circ$.

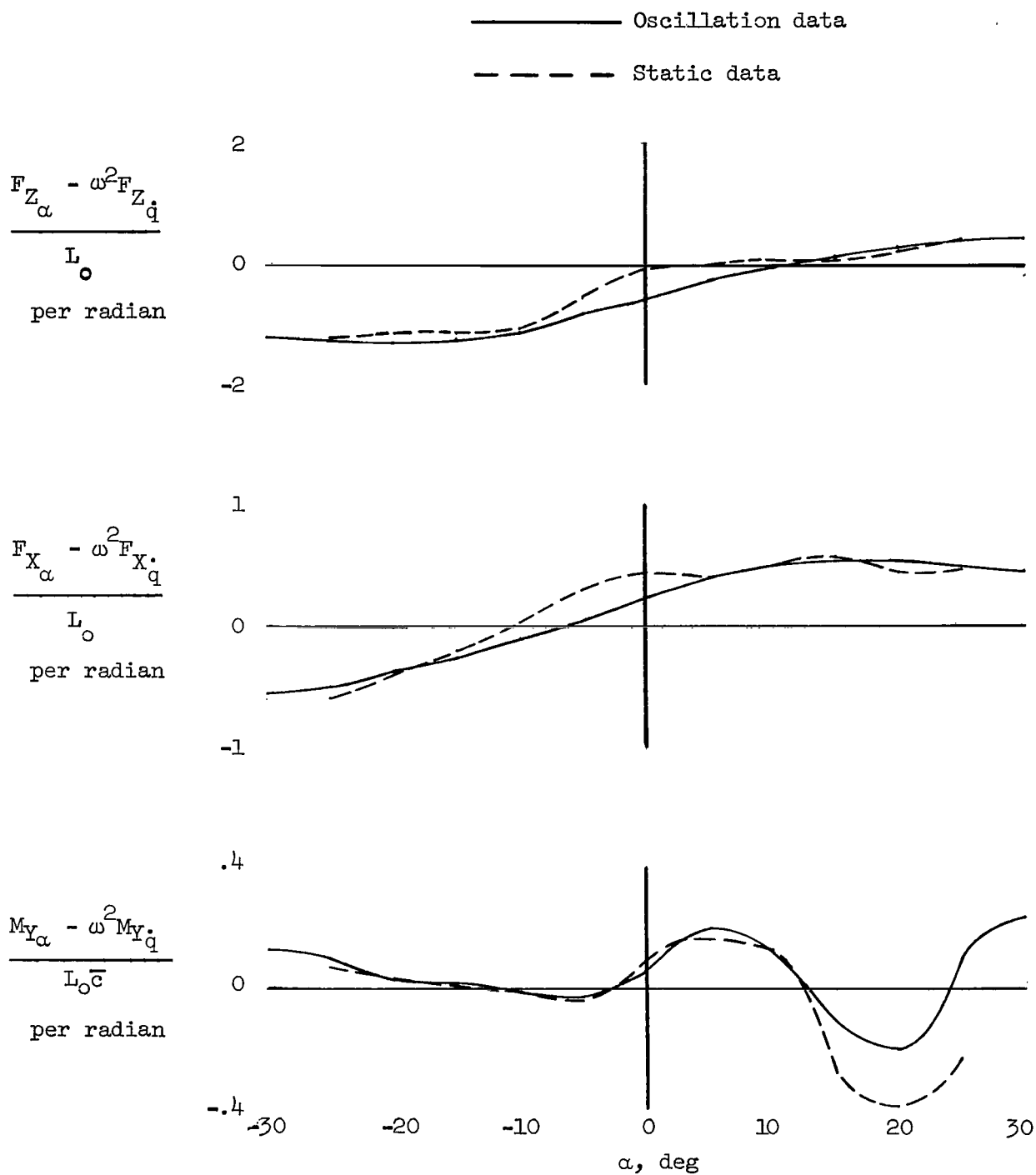


Figure 21.- Comparison of in-phase oscillatory and static data for $i_w = 25^\circ$.

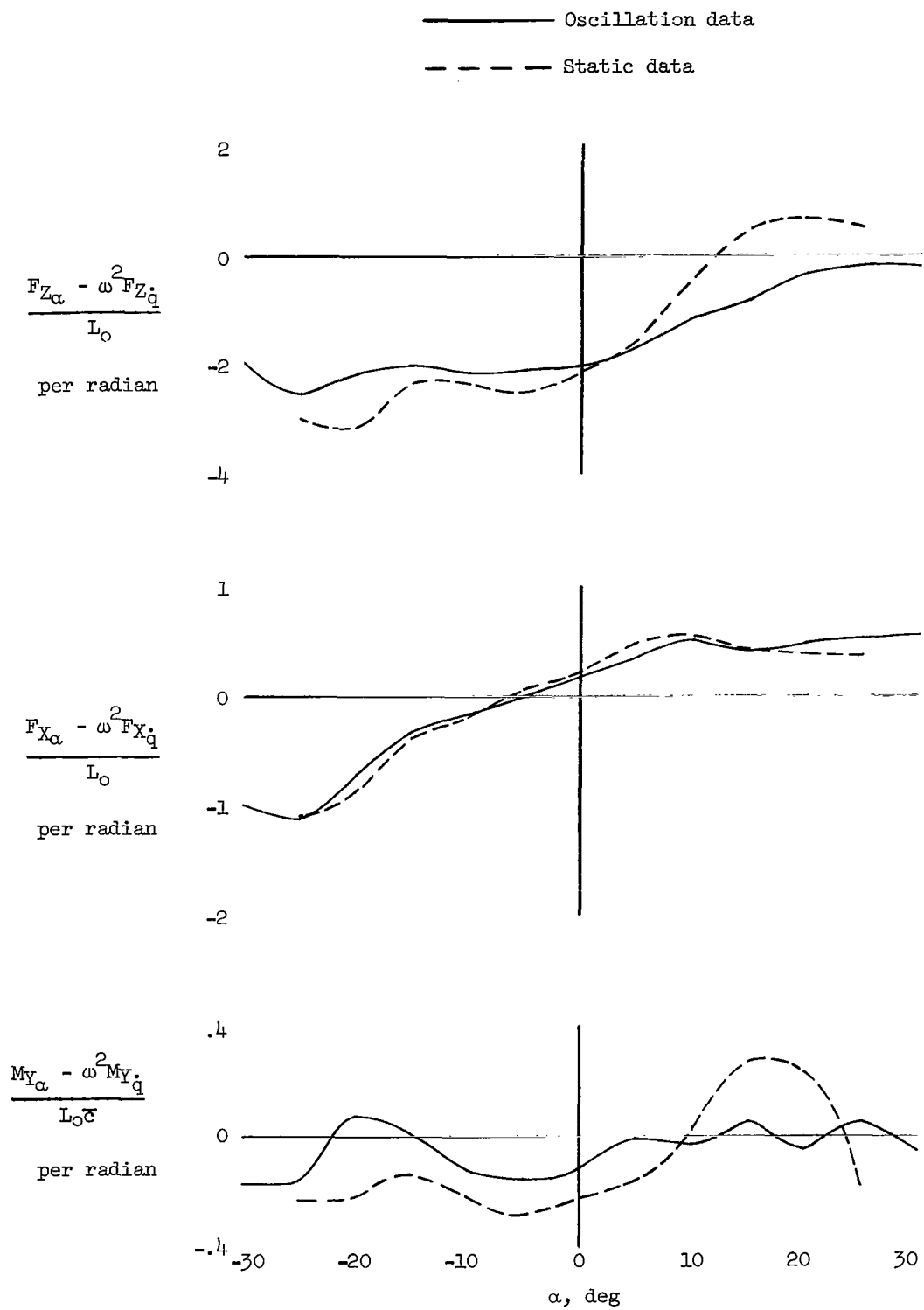


Figure 22.- Comparison of in-phase oscillatory and static data for $i_w = 10^\circ$.

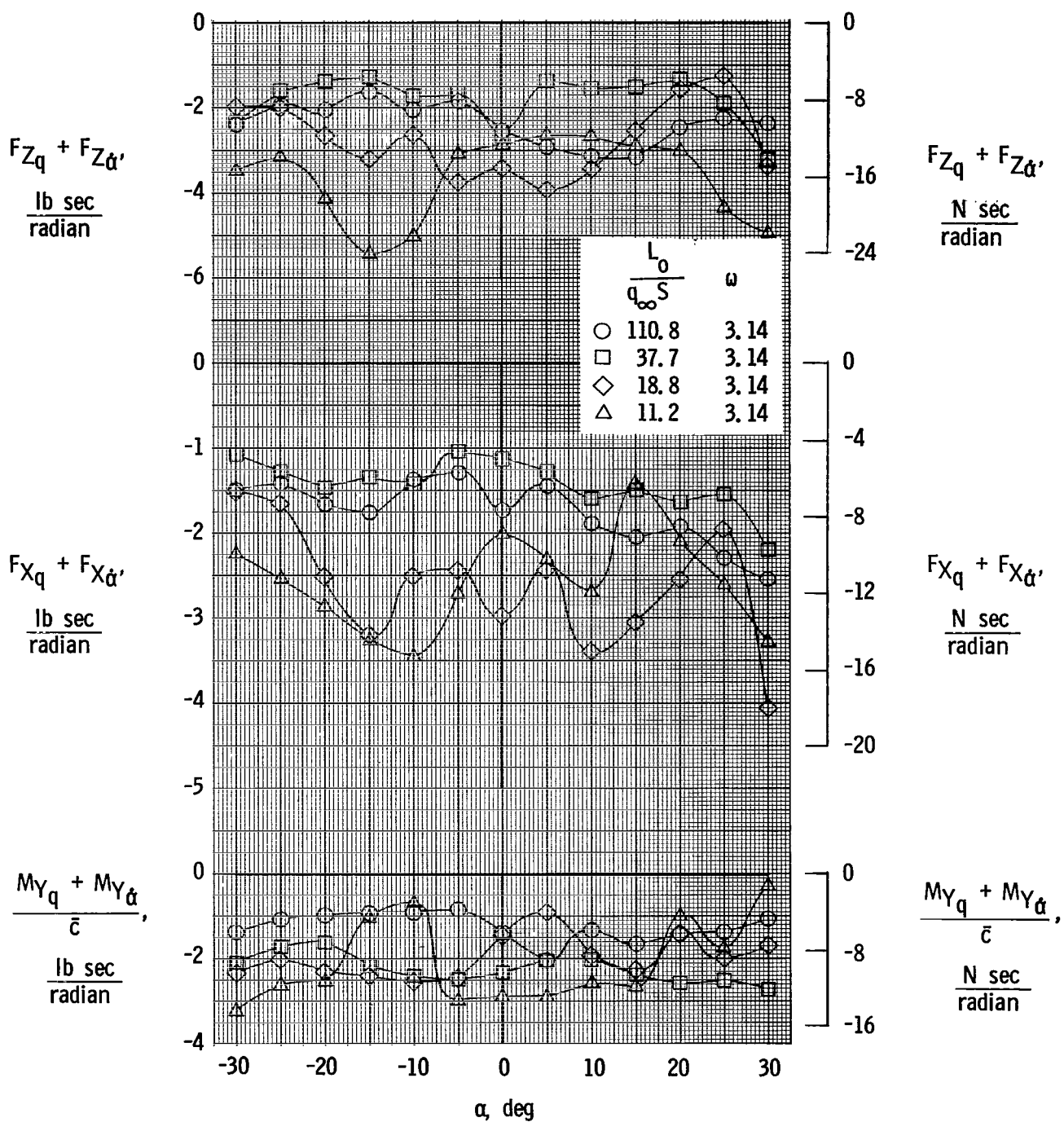


Figure 23.- Variation of out-of-phase oscillatory derivatives with angle of attack. $i_w = 65^\circ$; $i_t = 28^\circ$; $L_0 = 71.3$.

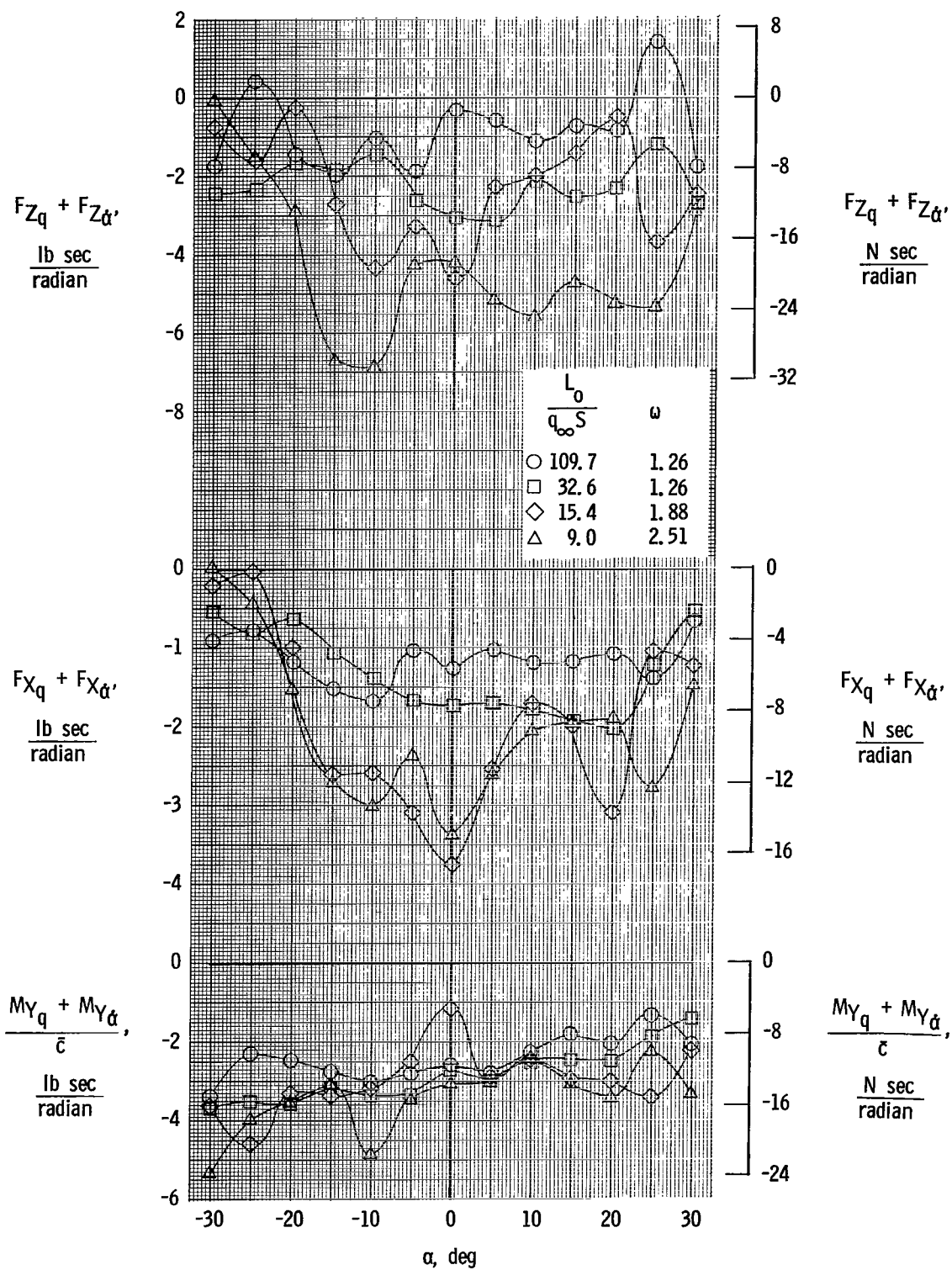


Figure 24.- Variation of out-of-phase oscillatory derivatives with angle of attack. $i_w = 50^\circ$; $i_t = 45^\circ$; $L_0 = 71.3$.

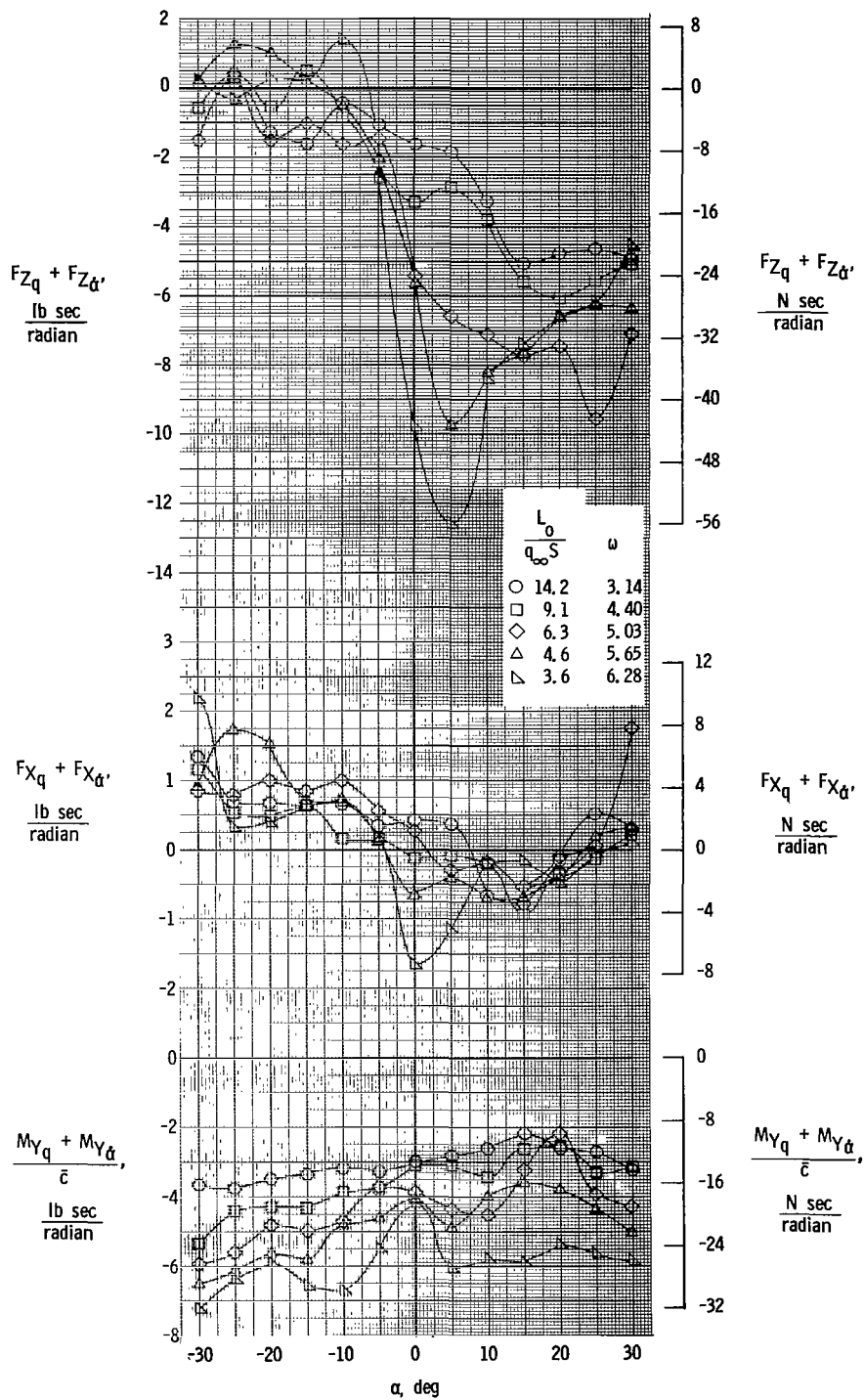


Figure 25.- Variation of out-of-phase oscillatory derivatives with angle of attack. $i_w = 25^\circ$; $i_t = 23^\circ$; $L_0 = 71.3$.

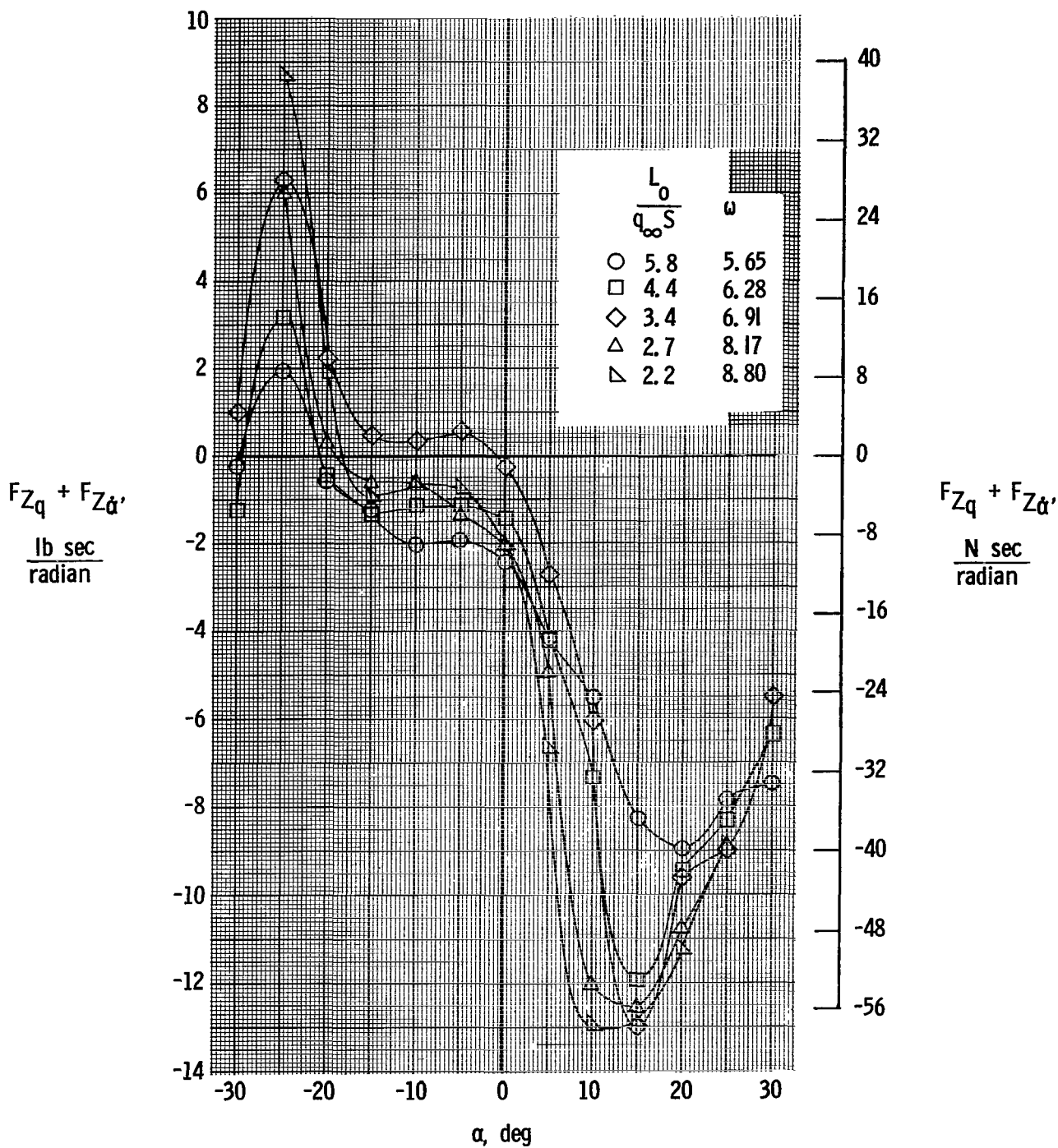


Figure 26.- Variation of out-of-phase oscillatory derivatives with angle of attack. $i_w = 10^\circ$; $i_t = 10^\circ$; $L_0 = 71.3$.

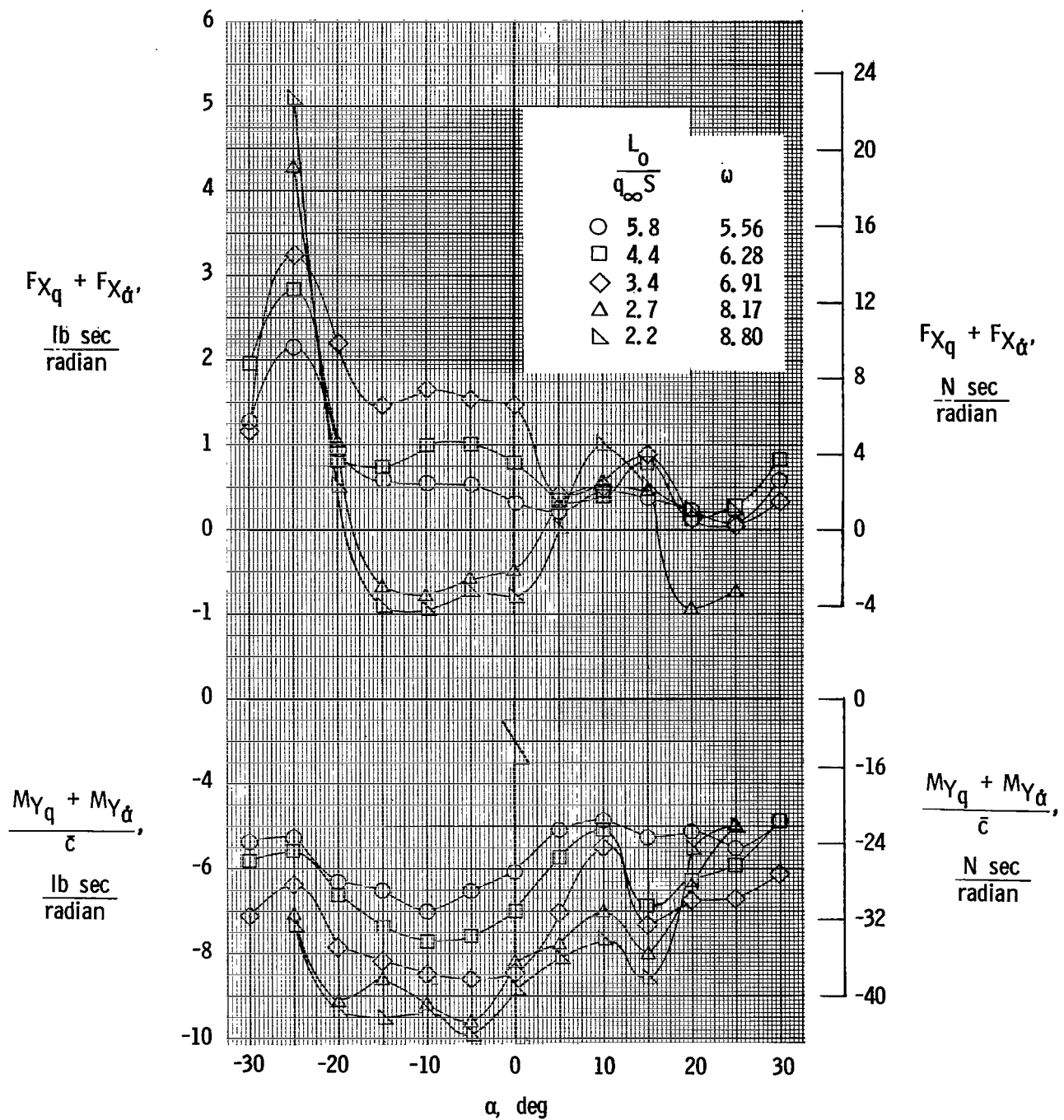


Figure 26.- Concluded.

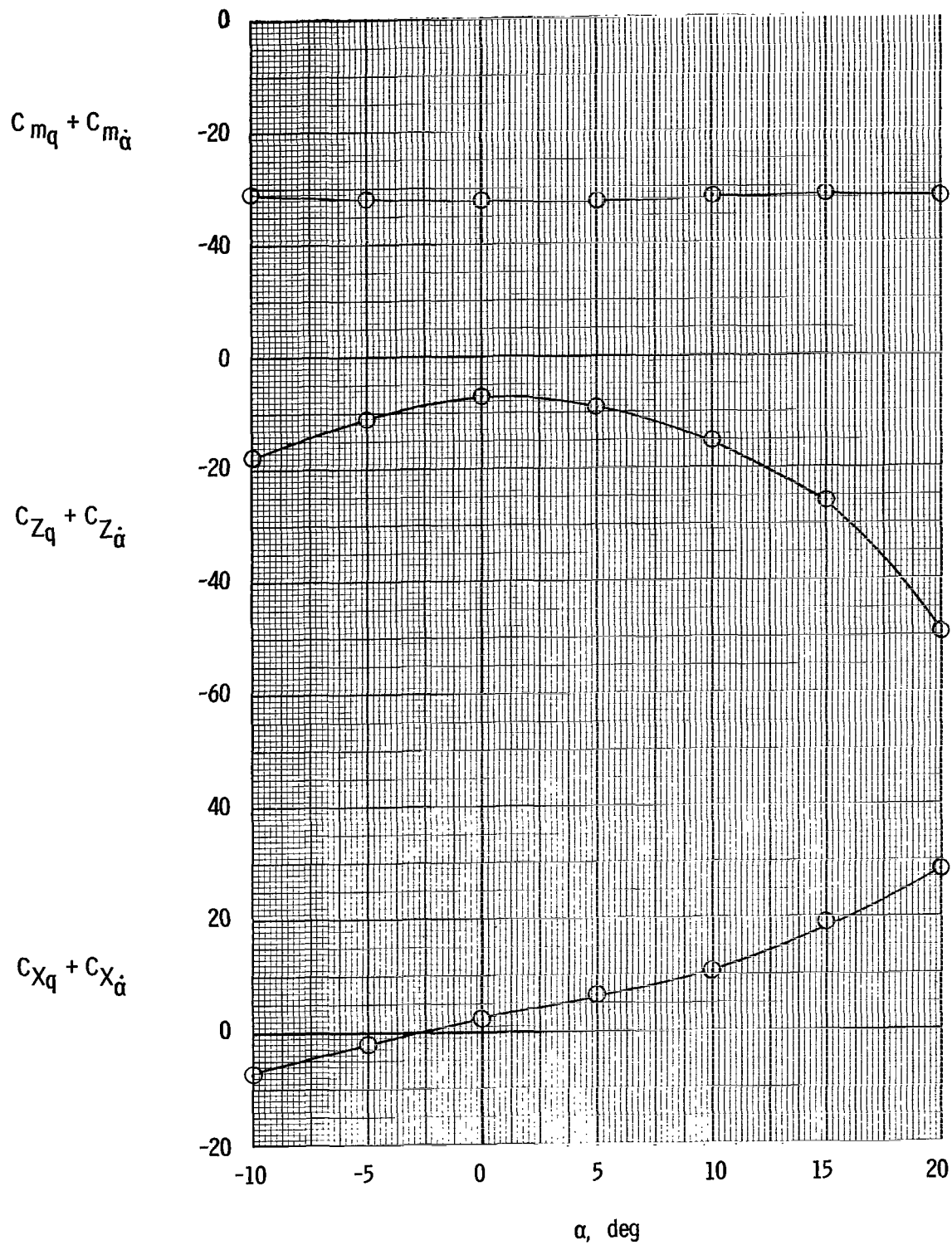


Figure 27.- Variation of out-of-phase oscillatory derivatives with angle of attack. $i_w = 0^\circ$; $i_t = 0^\circ$; propellers windmilling.

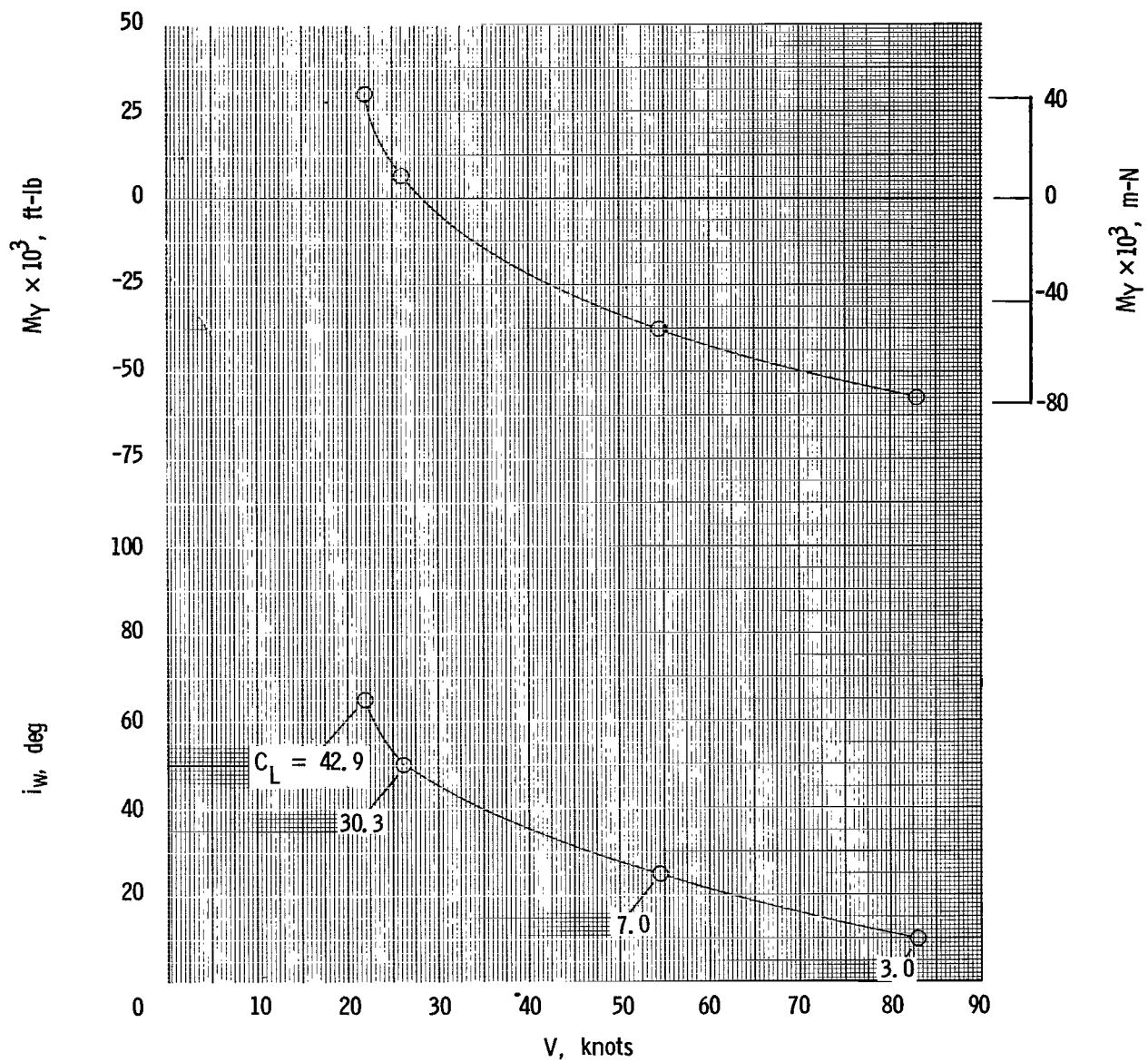


Figure 28.- Variation of static pitching moment and wing incidence with forward speed for full-scale airplane.
 $W/S = 70 \text{ lb/ft}^2$ (3352 N/m²); $\alpha = 0^\circ$.

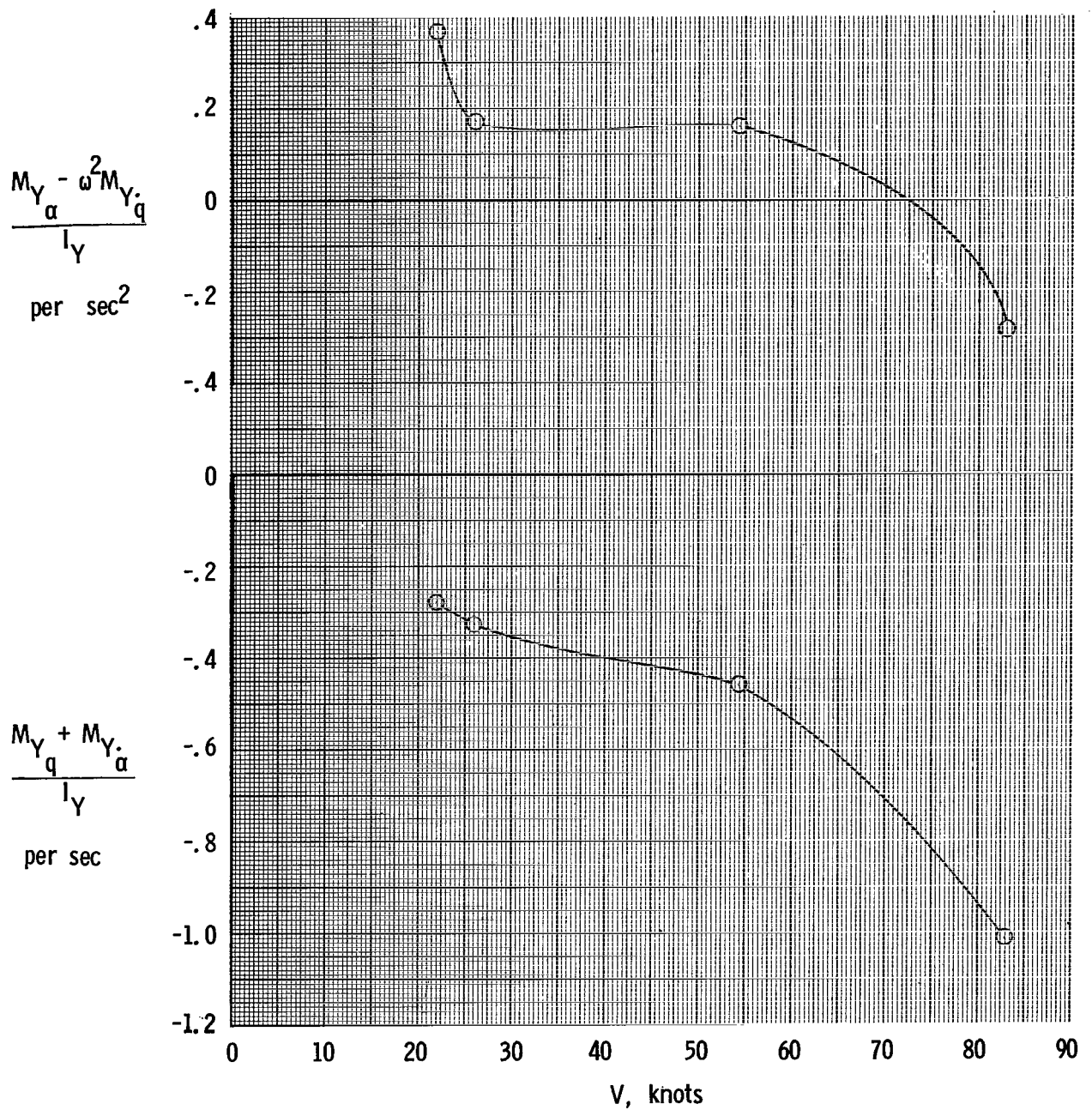


Figure 29.- Variation of static longitudinal stability parameter and damping-in-pitch parameter with forward speed for full-scale airplane.
 $W/S = 70 \text{ lb/ft}^2$ (3352 N/m²); $\alpha = 0^\circ$; $I_Y = 125\,000 \text{ slug-ft}^2$ (169 476 kg-m²).

"The aeronautical and space activities of the United States shall be conducted so as to contribute . . . to the expansion of human knowledge of phenomena in the atmosphere and space. The Administration shall provide for the widest practicable and appropriate dissemination of information concerning its activities and the results thereof."

—NATIONAL AERONAUTICS AND SPACE ACT OF 1958

NASA SCIENTIFIC AND TECHNICAL PUBLICATIONS

TECHNICAL REPORTS: Scientific and technical information considered important, complete, and a lasting contribution to existing knowledge.

TECHNICAL NOTES: Information less broad in scope but nevertheless of importance as a contribution to existing knowledge.

TECHNICAL MEMORANDUMS: Information receiving limited distribution because of preliminary data, security classification, or other reasons.

CONTRACTOR REPORTS: Technical information generated in connection with a NASA contract or grant and released under NASA auspices.

TECHNICAL TRANSLATIONS: Information published in a foreign language considered to merit NASA distribution in English.

TECHNICAL REPRINTS: Information derived from NASA activities and initially published in the form of journal articles.

SPECIAL PUBLICATIONS: Information derived from or of value to NASA activities but not necessarily reporting the results of individual NASA-programmed scientific efforts. Publications include conference proceedings, monographs, data compilations, handbooks, sourcebooks, and special bibliographies.

Details on the availability of these publications may be obtained from:

SCIENTIFIC AND TECHNICAL INFORMATION DIVISION
NATIONAL AERONAUTICS AND SPACE ADMINISTRATION
Washington, D.C. 20546